

AMEP: The Active Matter Evaluation Package for Python

Lukas Hecht,^{1,*} Kay-Robert Dormann,¹ Kai Luca Spanheimer,¹ Mahdiah Ebrahimi,¹ Malte Cordts,¹ Suvendu Mandal,¹ Aritra K. Mukhopadhyay,¹ and Benno Liebchen^{1,†}

¹*Institute for Condensed Matter Physics, Department of Physics,
Technische Universität Darmstadt, Hochschulstr. 8, 64289 Darmstadt, Germany*

(Dated: April 26, 2024)

The Active Matter Evaluation Package (AMEP) is a Python library for analyzing simulation data of particle-based and continuum simulations. It provides a powerful and simple interface for handling large data sets and for calculating and visualizing a broad variety of observables that are relevant to active matter systems. Examples range from the mean-square displacement and the structure factor to cluster-size distributions, binder cumulants, and growth exponents. AMEP is written in pure Python and is based on powerful libraries such as NumPy, SciPy, Matplotlib, and scikit-image. Computationally expensive methods are parallelized and optimized to run efficiently on workstations, laptops, and high-performance computing architectures, and an HDF5-based data format is used in the backend to store and handle simulation data as well as analysis results. AMEP provides the first comprehensive framework for analyzing simulation results of both particle-based and continuum simulations (as well as experimental data) of active matter systems. In particular, AMEP also allows it to analyze simulations that combine particle-based and continuum techniques such as used to study the motion of bacteria in chemical fields or for modeling particle motion in a flow field. AMEP is available at <https://amepproject.de> and can be installed via conda and pip.

I. INTRODUCTION

Computer simulations are a powerful method to investigate and understand the physical properties of soft matter and biological systems. In particular, molecular dynamics (MD) simulations stand out as an indispensable tool to determine the microscopic dynamics and structural properties of molecular systems comprising bio-molecules [1–3], polymer electrolytes [4–6], liquid crystals [7–9], or confined liquids [10–13] for example. These systems exhibit notable relevance in both industrial and medical applications [14–16]. Expanding beyond atomistic and systematically coarse-grained MD simulations involving suitable force fields, Brownian dynamics (BD) simulations have extensively been used over the past two decades especially also for modelling active matter systems. In such systems, the individual constituents consume energy from their environment and use it to self propel and navigate through complex surroundings [17, 18]. Examples of active matter systems can be observed across scales from microscopic entities such as bacteria, algae, and synthetic microswimmers [19–28] to fishes, birds, drones, and human crowds on the macroscale [29–37]. These out-of-equilibrium systems exhibit striking collective phenomena such as phase separation (where the system selects a density) [38–47], non-equilibrium pattern formation (where the system selects a length scale) [48–54], or other ordering transitions such as flocking showing (long-range) orientational ordering [35, 55–57].

To effectively model active matter systems, different computational approaches provide distinct advantages

[58, 59]. Particle-based models such as the active Brownian particle (ABP) model [60], solved numerically using BD simulations for example, have proven valuable for investigating collective phenomena such as motility-induced phase separation (MIPS) [38, 43, 61–73] as well as the dynamics and local order of the involved individual particles [19, 74–81]. Conversely, continuum models such as the active model B+ [82] enable us to understand collective phenomena over larger length and time scales by studying the evolution of particle densities [49, 52, 57, 66, 82–87]. Therefore, it is a common approach to start from a particle-based model and subsequently derive a continuum model via coarse-graining techniques [50, 56, 67, 88–95]. Moreover, the integration of particle-based and continuum models has emerged as a promising approach [24, 48, 96–101], especially for scenarios such as modeling the interaction of active particles with a surrounding fluid or another medium that is quasi-continuous on the scale of the considered particles, as exemplified by the motion of bacteria or synthetic Janus colloids in a self-produced concentration field [97–100, 102–104]. These approaches are also particularly important for modeling artificial microswimmers such as active colloids in the presence of chemical fields [105, 106], exhibiting phenomena such as chemotaxis [86, 98, 107, 108].

To gain physical insights from the data resulting from numerical solutions, a comprehensive array of analysis techniques is required. The mean-square displacement and time correlation functions such as the orientational autocorrelation function are popular observables to achieve insights into the dynamical aspects [78, 109–118], while spatial correlation functions such as the radial/pair distribution function and the structure factor are frequently considered to provide information about spatial structures [45, 119–122]. Other observables such

* lukas.hecht@pkm.tu-darmstadt.de

† benno.liebchen@pkm.tu-darmstadt.de

as entropy production and kinetic temperature are also considered frequently to analyze the collective behavior of the system under investigation [72, 73, 79, 123–139], and together with statistical analysis tools such as binder cumulants used in finite size scaling analyses [43, 140–143] and cluster analyses including cluster growth exponents [47, 72, 75, 89, 144–147], these observables allow us to characterize the non-equilibrium phase diagram and critical dynamics of active matter systems. Additionally, local order analyses such as local density and bond orientational order parameters offer insights into the system’s local structure and symmetries [43, 61, 62, 74, 148–151]. While existing analysis packages such as `freud` [152], `MDAnalysis` [153, 154], `VMD` [155], `MDTraj` [156], `Ovito` [157], `Pytim` [158], `LOOS` [159, 160], and `MMTK` [161] offer the possibility to calculate such observables, they are mostly inspired by and optimized for the MD simulation community and fall short in capturing all relevant observables for active matter systems in a single package. Additionally, they lack the possibility to handle continuum simulation data. Therefore, a new library is required that (i) consolidates the essential observables needed to analyze active matter simulation data, (ii) provides a unified platform for analyzing both particle-based and continuum simulation data, and (iii) seamlessly integrates data formats widely-used in computational physics through an application programming interface (API).

In this paper, we introduce the Active Matter Evaluation Package (`AMEP`), a unified framework for analyzing MD simulation, BD simulation, and continuum simulation data with a specific focus on soft and active matter systems. `AMEP` provides an optimized framework for loading, storing, and evaluating simulation data based on particle trajectories and the time evolution of continuum fields. This framework is based on an optimized HDF5 file format [162, 163] which is optimal for long-term storage purposes and for handling data of large-scale simulations [163–165]. Computationally expensive methods are parallelized and `AMEP` selectively loads only the data into the main memory which is necessary for the current computational step. This ensures efficient operation on high-performance computing architectures, workstations, and laptops. `AMEP` is written in pure Python and provides a user-friendly, easy-to-learn Python API that interfaces with common tools used in computational physics via NumPy arrays [166, 167]. Based on common Python libraries such as NumPy [166, 167], SciPy [168], Matplotlib [169], and scikit-image [170], `AMEP` provides a powerful toolbox for calculating spatial and temporal correlation functions, visualizing and animating simulation results, and coarse-graining particle-based simulations, which makes it possible to easily analyze the dynamics and structure of both particle-based and continuum simulation data.

The paper is organized as follows: We first demonstrate a minimal example on how to use `AMEP` to load, analyze, and visualize simulation data in Section II. Second, we give a brief overview on the structure and design

of `AMEP` in Section III. Finally, in Sections IV and V, we apply a selection of analysis functions provided by `AMEP` to particle-based simulations of the ABP model and to continuum simulations of the active model B+, respectively, and briefly discuss the results.

II. HOW TO USE AMEP

`AMEP` is designed with a user-focused mindset to simplify the access to simulation data within a few lines of Python code. Before discussing the general design of `AMEP` and various examples on how to apply it to particle-based and continuum simulation data, we will demonstrate its general usage with a minimal example. For a quick start with `AMEP`, we recommend to download the demo files at <https://github.com/ameproject/amep/tree/main/examples> and to run them part by part while reading this section.

A. Exemplary data: The active Brownian particle model

Within the following example, we load simulation data from a particle-based simulation of the overdamped active Brownian particle (ABP) model in two spatial dimensions. The ABP model is one of the simplest and most popular models to describe active particles that self-propel in a certain direction which smoothly changes due to rotational diffusion [47, 59, 60, 62, 72, 74, 75, 114, 171, 172]. Within this model, each particle is represented by a (slightly soft) disk/sphere of diameter σ , mass m , and moment of inertia I and possesses an inherent internal drive, denoted by an effective self-propulsion force $\vec{F}_{\text{SP},i} = \gamma_t v_0 \hat{p}(\theta_i)$, where the self-propulsion direction is represented by $\hat{p}(\theta_i) = (\cos \theta_i, \sin \theta_i)$ and v_0 denotes the terminal self-propulsion speed. The interactions between the particles are governed by an excluded-volume repulsive interaction potential u . The evolution of the particles’ positions \vec{r}_i and orientations θ_i adheres to the Langevin equations [72, 73, 114, 139, 171]

$$m \frac{d^2 \vec{r}_i}{dt^2} = -\gamma_t \frac{d\vec{r}_i}{dt} - \sum_{\substack{j=1 \\ j \neq i}}^N \nabla_{\vec{r}_i} u(r_{ji}) + \gamma_t v_0 \hat{p}(\theta_i) + \sqrt{2k_B T_b \gamma_t} \vec{\eta}_i(t), \quad (1)$$

$$I \frac{d^2 \theta_i}{dt^2} = -\gamma_r \frac{d\theta_i}{dt} + \sqrt{2k_B T_b \gamma_r} \xi_i(t). \quad (2)$$

Here, $\vec{\eta}_i$ and ξ_i denote Gaussian white noise with zero-mean and unit variance, T_b represents the bath temperature, γ_t and γ_r denote the translational and rotational drag coefficients, respectively, k_B is the Boltzmann constant, and N denotes the total number of active particles. The overdamped limit can be obtained using $m/\gamma_t \rightarrow 0$ and $I/\gamma_r \rightarrow 0$ (see also Section IV).

B. Installing AMEP

AMEP is a Python library that requires Python 3.10 or higher. To use AMEP, we recommend to install Python via Anaconda¹. If Anaconda is installed, one can create a new environment, activate it, and install AMEP through the terminal (Linux/macOS) or the Anaconda Prompt (Windows):

```
1 conda create -n amepenv python=3.10
2 conda activate amepenv
3 conda install conda-forge::amep
```

Now, one can start the Python interpreter to import and use AMEP:

```
4 python
5 >>> import amep
6 >>>
```

Alternatively, we recommend to use Jupyter notebooks².

C. Analyzing simulation data using AMEP

Now, we use AMEP to calculate the mean-square displacement (MSD), the diffusion coefficient, and the orientation autocorrelation function (OACF) of a single ABP and the radial distribution function (RDF) of multiple interacting ABPs. At the end of this section, we visualize the results in a combined plot. Exemplary code and data of the relevant ABP simulations is available at <https://github.com/amepproject/amep/tree/main/examples>.

First, we import AMEP and load the simulation data of non-interacting overdamped ABPs:

```
1 import amep
2 traj_nonint = amep.load.traj(
3     "/path/to/non_interacting_ABPs",
4     mode = "lammmps"
5 )
```

The function `amep.load.traj` creates an HDF5 file (`traj.h5amep`) in the background that contains all the simulation data and returns a `ParticleTrajectory` object which allows to easily access the data for further processing. Since the data has been produced using LAMMPS [173], we load it using `mode = "lammmps"`. To save useful information for long-term storage, we add the author to the trajectory object, which will save this information within the linked HDF5 file:

```
6 traj_nonint.add_author_info(
7     "Lukas Hecht",
8     "affiliation",
9     "Technical University of Darmstadt"
10 )
11 traj_nonint.add_author_info(
12     "Lukas Hecht",
13     "email",
14     "lukas.hecht@pkm.tu-darmstadt.de"
15 )
```

This information can be accessed by calling `traj_nonint.get_author_info("Lukas Hecht")`, returning

```
{'affiliation': 'Technical University of Darmstadt',
'email': 'lukas.hecht@pkm.tu-darmstadt.de'}
```

while `traj_nonint.authors` returns a list of all authors. AMEP provides several methods to add more information to trajectory objects (`ParticleTrajectory` or `FieldTrajectory`) such as software information, simulation scripts, log files, or simulation parameters for a comprehensive and reproducible set of information about the simulation (see online documentation available at <https://amepproject.de> and Fig. 1).

Next, we calculate the MSD, which is defined as

$$\text{MSD}(t) = \frac{1}{N} \sum_{i=1}^N [\vec{r}_i(t) - \vec{r}_i(0)]^2, \quad (3)$$

where $\vec{r}_i(0)$, $\vec{r}_i(t)$ denote the position of particle i at time 0 and $t \geq 0$, respectively. For a single ABP, it can be shown analytically that the MSD can be written as

$$\text{MSD}(t) = 2l_p^2 \left(\frac{t}{\tau_p} - 1 + e^{-t/\tau_p} \right) + 4D_t t \xrightarrow{t \gg \tau_p} 4D_{\text{eff}} t \quad (4)$$

with effective diffusion coefficient $D_{\text{eff}} = D_t + l_p^2/(2\tau_p)$ [23, 59, 174]. Here, $\tau_p = 1/D_r$ denotes the persistence time, which signifies the time after which the directed motion of an ABP is randomized due to rotational diffusion, and $l_p = v_0\tau_p$ denotes the persistence length, which is the distance an ABP moves on average before its direction of motion is randomized. $D_t = k_B T_b / \gamma_t$ and $D_r = k_B T_b / \gamma_r$ are the translational and rotational diffusion coefficients, respectively, and v_0 is the terminal self-propulsion speed of the ABP. To calculate the MSD with AMEP, we create a `MSD` object via

```
16 msd = amep.evaluate.MSD(
17     traj_nonint
18 )
```

which calculates the MSD for all frames and performs the average over all particles. The `MSD` object contains all information about the MSD and we can access the times via `msd.times` and the value for each individual frame via `msd.frames` for example. The returned objects are NumPy arrays and can therefore easily be used also elsewhere in Python.

To get the effective diffusion coefficient D_{eff} from the MSD in the late time limit, we define the fit function `f` with the fit parameters as keyword arguments and create a corresponding `Fit` object:

```
19 def f(t, D = 1.0):
20     return 4*D*t
21 Dfit = amep.functions.Fit(f)
```

By calling the object's `fit` method, which uses the `scipy.odr` package in the background, with the data to fit and an initial guess (using the `p0` keyword), we obtain the optimal parameters. Here, we only want to fit the long-time behaviour, and hence, we only consider data for $t > 10^1 \tau_p$. The optimal parameters and their errors can then be retrieved from the `Fit` object:

¹ See <https://docs.anaconda.com/free/anaconda/install/index.html> for instructions on how to install Anaconda.

² For more information about Jupyter notebooks, see <https://jupyter.org/>.

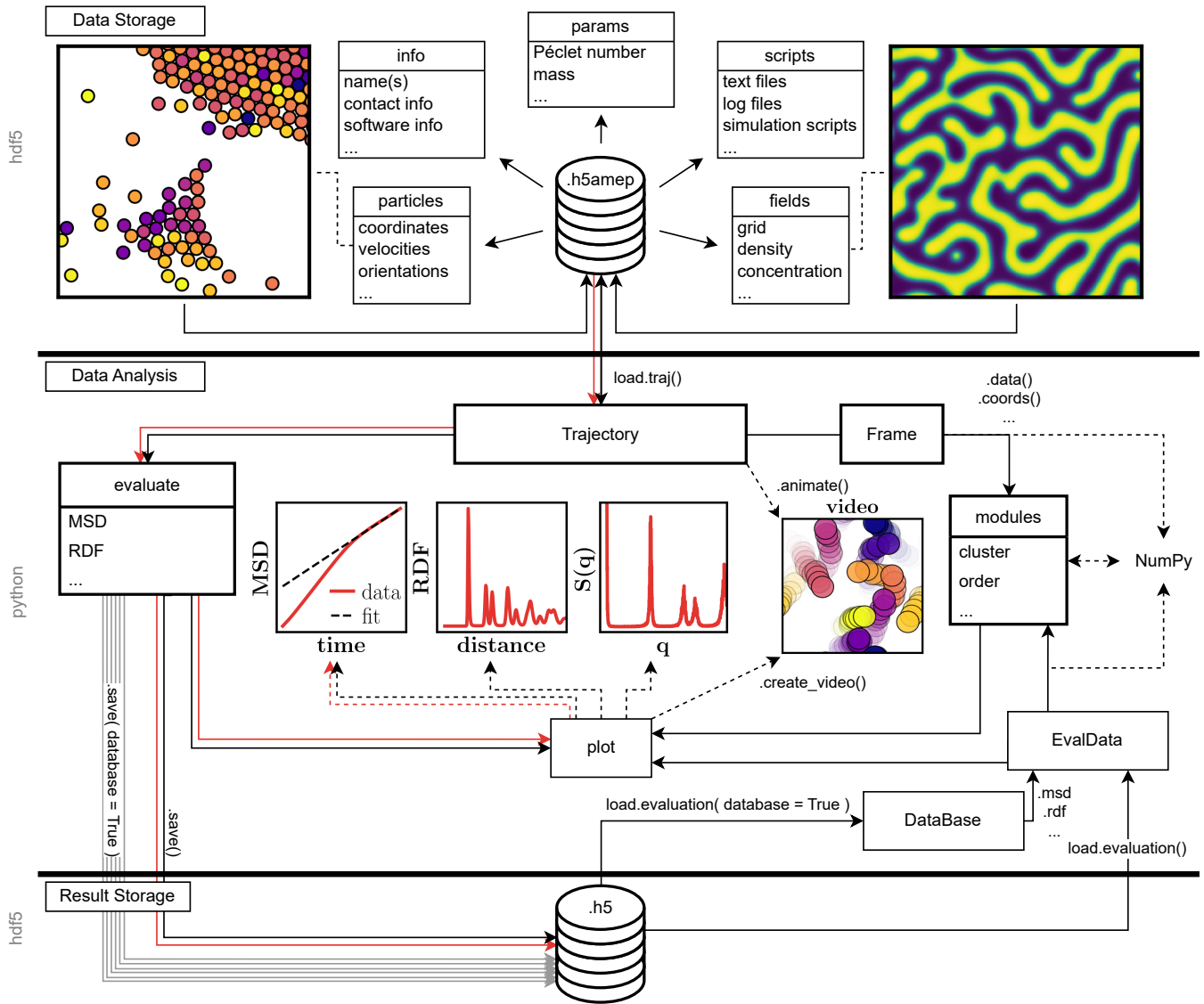


Figure 1. AMEP flow chart: Schematic of the design of AMEP. The first layer “Data Storage” represents the loading and storage of data from particle-based or continuum simulations, which is stored in HDF5 files (`.h5amep`) together with various metadata the user can add. The central part of the Python interface (layer “Data Analysis”) is the `Trajectory` object which acts as a list of `Frame` objects and gives access to the data stored in the HDF5 file. The `Trajectory` object can be used with the evaluate classes (module `evaluate`) which give simple access to many observables calculated over whole trajectories. Alternatively, the data can be returned as NumPy array through the `Frame` objects and can be analyzed using the individual AMEP modules, also in combination with self-written Python code to perform additional operations beyond AMEP. The `plot` module allows to visualize analysis results and simulation data in form of figures or videos. Finally, the results can be stored in an HDF5-based data format again (layer “Result Storage”). It is possible to save and load one or more results in one HDF5 file. Later, the results can be imported as `DataBase` (for multiple results) or `EvalData` objects (one result in a file or one result selected from a `DataBase` object). The red arrows follow the path of our first minimal example as discussed in Section II. The design itself is explained in more detail in Section III.

```

22 mask = msd.times > 1e1
23 Dfit.fit(
24     msd.times[mask],
25     msd.frames[mask],
26     p0 = [900]
27 )
28 print(
29     f"D={Dfit.params[0]:0.2f}, \"
30     f"D-error={Dfit.errors[0]:0.2f}\"
31 )

```

D=885.32, D-error=0.59

This is fairly close to the expected value of $D_{\text{eff}} = 883$ as obtained from Eq. (4) for ABPs with $l_p = 1.0$, $\tau_p = 1.0$, $v_0 = 42$, and $D_t = 1.0$ as used in this example.

Next, we use the same simulation data to calculate and

fit the OACF, which is given by

$$\langle \hat{p}(0) \cdot \hat{p}(t) \rangle = \frac{1}{N} \sum_{i=1}^N \hat{p}_i(0) \cdot \hat{p}_i(t) \quad (5)$$

and is equal to $e^{-D_r t}$ for overdamped ABPs [114]. Here, \hat{p}_i is the orientation vector of the effective self-propulsion force of particle i . Again, by creating the corresponding evaluate and fit objects, we can analyze the OACF in a few lines of Python code. For the correct normalization, we specify the plane in which the OACF is to be calculated with `direction = "xy"`:

```
32 oacf = amep.evaluate.OACF(
33     traj.nonint,
34     direction = "xy"
35 )
36 def f(t, Dr = 1.0):
37     return np.exp(-Dr*t)
38 Tfit = amep.functions.Fit(f)
39 Tfit.fit(oacf.times, oacf.frames)
40 print(
41     f"Dr={Tfit.params[0]:0.4f}, "\
42     f"Dr-error={Tfit.errors[0]:0.4f}"
43 )
```

Dr=0.9890, Dr-error=0.0021

Again, we obtain a value close to the expected one of $D_r = 1.0$.

Next, we calculate the RDF. For that, we load simulation data of $N = 10^5$ interacting ABPs moving in a two-dimensional periodic simulation box with a total packing fraction of $\varphi = 0.5$ and create a RDF evaluate object. Note that a corresponding exemplary dataset is available at <https://github.com/amepproject/amep/tree/main/examples>. Here, we only want to consider frames that are in the steady state. Therefore, we skip the first 90 % of frames using `skip = 0.9`. Additionally, we specify the total number of frames to average over (time average) equally spaced in time over the last 90 % of the trajectory using the `nav` keyword, which is inherited from the `BaseEvaluation` class and is short for “number of averages”. Due to the large number of particles, it is worth to use multiprocessing, to set a maximum distance until which the RDF is calculated, and to use a large number of bins using the `njobs`, `rmax`, and `nbins` keywords, respectively:

```
44 traj_int = amep.load.traj(
45     "/path/to/interacting_ABPs",
46     mode = "lammps"
47 )
48 rdf = amep.evaluate.RDF(
49     traj_int,
50     skip = 0.9,
51     nav = 100,
52     nbins = 20000,
53     rmax = 300,
54     njobs = 128
55 )
```

Before visualizing the results, we save them in HDF5 files. For that, AMEP offers two possibilities: One can store the result of either a single evaluate object (as done for the RDF) or multiple evaluate objects (as done for the MSD and the OACF) in one HDF5 file:

```
56 msd.save(
57     "nonint-results.h5",
58     database = True
```

```
59 )
60 oacf.save(
61     "nonint-results.h5",
62     database = True
63 )
64 rdf.save(
65     "rdf.h5"
66 )
```

These can later be loaded by calling `msd = amep.load.evaluation("nonint-results.h5", database = True).msd` and `rdf = amep.load.evaluation("rdf.h5")` for example.

Finally, the data and fits can be visualized with the Matplotlib wrappers provided by AMEP (Fig. 2):

```
67 fig, axs = amep.plot.new(
68     (6.5,2), ncols = 3, wspace = 0.1
69 )
70 # plot msd
71 axs[0].plot(
72     msd.times, msd.frames,
73     "r-", label = "data"
74 )
75 axs[0].plot(
76     msd.times, Dfit.generate(msd.times),
77     "k--", label = "fit"
78 )
79 axs[0].set_xlabel("Time")
80 axs[0].set_ylabel("MSD")
81 axs[0].loglog()
82 axs[0].legend()
83
84 # plot oacf
85 axs[1].plot(
86     oacf.times, oacf.frames,
87     "r-", label = "data"
88 )
89 axs[1].plot(
90     oacf.times, Tfit.generate(oacf.times),
91     "k--", label = "fit"
92 )
93 axs[1].set_xlabel("Time")
94 axs[1].set_ylabel("OACF")
95 axs[1].semilogx()
96 axs[1].axhline(1/np.e, c = "k")
97 axs[1].axvline(1, c = "k")
98 axs[1].legend()
99
100 # plot rdf
101 axs[2].plot(rdf.r, rdf.avg, "r-")
102 axs[2].semilogx()
103 axs[2].set_xlabel("Distance")
104 axs[2].set_ylabel("RDF")
105
106 # plot boxes
107 amep.plot.draw_box(
108     fig, [0, 0, 0.68, 1.01],
109     edgecolor = "tab:blue", linestyle = "--",
110     text = "Single ABP", c = "tab:blue"
111 )
112 amep.plot.draw_box(
113     fig, [0.69, 0, 0.31, 1.01],
114     edgecolor = "tab:orange", linestyle = "--",
115     text = "Interacting ABPs", c = "tab:orange"
116 )
117 # save figure in file
118 fig.savefig("how.to.use.amep.pdf")
```

The whole workflow of this minimal example is marked with red arrows in the flowchart shown in Fig. 1 and its code is available at <https://github.com/amepproject/amep/tree/main/examples>.

III. DESIGN

In the previous section, we introduced a short example of how to use AMEP. We will now give an overview of the

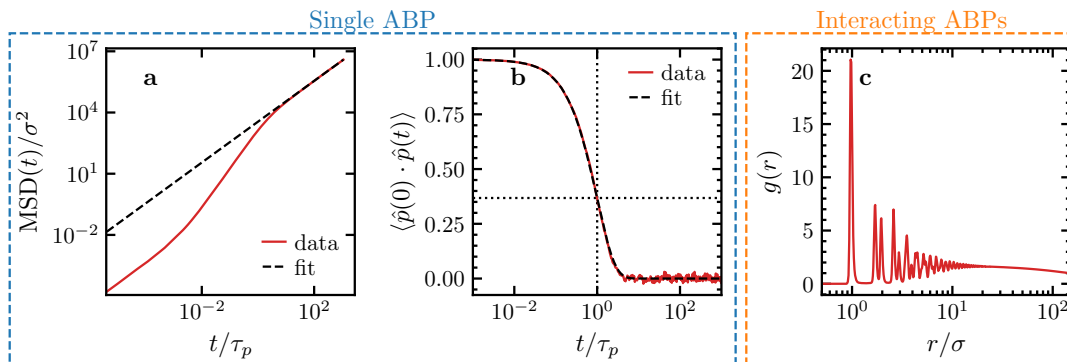


Figure 2. **How-to-use-AMEP example.** **a** Mean-square displacement of a single ABP calculated with `amep.evaluate.MSD`. The black dashed line is a fit of Eq. (4) done with `amep.functions.Fit`. **b** Orientation autocorrelation function of a single ABP calculated with `amep.evaluate.OACF`. The black dashed line is a fit of $e^{-D_r t}$ done with `amep.functions.Fit` and the black dotted lines mark the point $(1, 1/e)$. The results in panels a and b are averaged over 4×10^3 particles. **c** Radial pair distribution function of $N = 10^5$ repulsively interacting ABPs calculated using `amep.evaluate.RDF` and averaged over time in the steady state. The plot has been created using the `amep.plot` module and the corresponding code is available at <https://github.com/ameproject/amep/tree/main/examples>.

design of the AMEP package. A more detailed description can be found in the online documentation available at <https://ameproject.de>.

A. Modules

AMEP contains a plethora of pre-implemented functions to analyze particle-based and continuum simulation data. In Tab. I, the modules are listed with a short description and a few exemplary functions. The functions contained in these modules take NumPy arrays and native Python data types as input and therefore, can also be used without the data-handling framework provided by AMEP. In addition to the modules shown in Tab. I, AMEP has a `plot` module to visualize simulation data and results as well as an `evaluate` module, which provides various evaluation methods that use a full trajectory as input data. The `plot` and the `evaluate` module will be described in more detail below.

B. Visualization

For visualizing simulation data and analysis results, AMEP provides the `plot` module, which is a wrapper for the Matplotlib library [169]. The `plot` module includes functions to plot particles and continuum fields (cf. Figs. 3 and 8), to create insets and colorbars (cf. Fig. 3), and to animate plots and simulation data (cf. Movies S1–S3, Supplemental Material). For example, a video of a trajectory `traj` can be created via `traj.animate("video.mp4")`. By varying the file extension, also other data formats can be used such as GIFs. Additionally, the `plot` module provides useful functions to format the axis of a figure. All visualization functions are optimized to create figures

and videos that can be directly used for a publication in various journals. All figures within this paper with the exception of Fig. 1 are created with AMEP.

C. Evaluate module

We already introduced the different modules of AMEP, which contain a plethora of functions relevant for the analysis of active matter simulation data. The `evaluate` module is a special module in the sense that it uses functions from all other modules to calculate certain observables for a whole trajectory. In our first example in Section II, we already used the `MSD`, `OACF`, and `RDF` classes, which are part of the `evaluate` module. We will now introduce the concept of these classes, which will be referred to as “evaluate classes” in the following.

While the functions of the modules discussed above take NumPy arrays as input data, evaluate classes take a whole trajectory as an input. One example is the `amep.evaluate.RDF` class used in Section II. To initialize an object of an evaluate class, the trajectory as well as certain parameters are supplied. The evaluate classes offer the functionality to average over multiple frames automatically (the keyword `nav`, which is an abbreviation for “number of averages”, allows to specify the number of frames to average over) as well as to skip a certain amount of frames at the beginning of the trajectory (in percent) by specifying the `skip` keyword. The resulting data can be returned as NumPy arrays. Furthermore, one or more evaluate objects can be stored in HDF5 files using their `.save("filename.h5")` method and can be read again with `amep.load.evaluation("filename.h5")`. The evaluate classes are a crucial part in the user-focused design of AMEP and make it possible to achieve results within a few lines of code.

D. File format

Based on the Hierarchical Data Format version 5 (HDF5) [162, 163], AMEP introduces a new file format `h5amep` to store simulation data and additional meta-data. This format is used in the backend of AMEP. The HDF5 files are structured into groups and datasets. The `h5amep` format has the following groups, subgroups, and attributes:

```
h5amep root
\amep
\info
  \authors
  \software
\scripts
\param
\type
\particles or \fields
\frames
  \steps
  \times
  \[frame0]
    \coords
    \velocities
    \...
  \[frame1]
    \...
  \...
```

The group `amep` contains information about the AMEP version that has been used to create the `h5amep` file. The group `info` contains the saved information about authors (cf. Section II) and software. The `scripts` group gives the possibility to save text files such as simulation scripts and log files that correspond to the simulation data. In the `params` group, AMEP stores parameters such as the simulation timestep for example. Additional simulation parameters can be added. The attribute `type` contains a flag about the type of data stored in the `h5amep` file. This can be either `"particle"` or `"field"`. The groups `particles` and `fields` contain user-defined information about the particles and the fields used in the simulation, respectively. Finally, the group `frames` contains multiple datasets and subgroups with the simulation data. The dataset `steps` stores a list of all the frame numbers (i.e., the number of timesteps for each frame) and the dataset `times` the corresponding (physical) time, while the individual frames of the simulation are stored in subgroups of `frames` named by their simulation step. Within an individual frame, the simulation data is stored, e.g., coordinates and velocities for particle-based simulations or density and concentrations for continuum simulations, as separate datasets.

E. Trajectories and frames

The `h5amep` file is connected to Python via the `amep.load` module with which the simulation data is imported to a `ParticleTrajectory` or `FieldTrajectory` object.

Table I. **Module overview.** The shown AMEP modules take NumPy arrays and native Python data types as input. The description of each module is complemented with a few exemplary functions (italic text). AMEP additionally provides the modules `plot` and `evaluate` as described in Section III. A detailed description of all modules and the contained functions can be found in the AMEP online documentation available at <https://amepproject.de>.

Module:	Description:
<code>cluster</code>	cluster identification and properties <i>identify clusters (particles)</i> <i>radius of gyration</i>
<code>continuum</code>	field data analysis and coarse-graining <i>identify clusters (fields)</i> <i>create field from particles</i>
<code>functions</code>	mathematical functions and fitting <i>Gaussian</i> <i>general fit class</i>
<code>order</code>	functions to characterize spatial order <i>local density</i> <i>k-atic bond order parameter</i>
<code>pbcc</code>	handling of periodic boundary conditions <i>create periodic images</i> <i>fold coordinates back into the box</i>
<code>spatialcor</code>	spatial correlation functions <i>radial distribution function</i> <i>isotropic structure factor</i>
<code>statistics</code>	methods for statistical analysis <i>binder cumulant</i> <i>distribution (histograms) 1d, 2d</i>
<code>thermo</code>	thermodynamic observables <i>kinetic temperature</i> <i>kinetic energies</i>
<code>timecor</code>	time correlation functions <i>mean squared distance</i> <i>autocorrelation function</i>
<code>utils</code>	utility methods <i>averaging methods (running mean, ...)</i> <i>Fourier transform</i>

Saved evaluation objects can also be imported with the `amep.load` module. Because a `ParticleTrajectory` or `FieldTrajectory` object works as a reader for the `h5amep` file, the simulation data (coordinates, velocities, density, concentration,...) is not stored in the main memory all the time but only the portion that is requested for the specific analysis. The simulation data can be accessed via `BaseFrame` or `BaseField` objects for particle-based and continuum data, respectively, which will be referred to as “frame” in the following. Technically, the `ParticleTrajectory` or `FieldTrajectory` object acts as a list of frames, i.e., `frame = traj[0]` returns the first frame of the trajectory `traj`. The data of one frame can be accessed through various methods. For example, the coordinates and velocities of particles can be accessed via `frame.coords()` and `frame.velocities()`. Other data can be accessed via the `frame.data` method, e.g., `frame.data("mass")` returns the mass of each particle and `frame.data("rho")` the density field of a continuum simulation. A list of all

available keys can be accessed via `frame.keys`. All these methods return NumPy arrays for efficient calculations and simple integrity to other Python packages (see also Fig. 1).

IV. ANALYZING PARTICLE-BASED SIMULATION DATA WITH AMEP

We will now use AMEP to analyze simulation data of large-scale simulations of ABPs. After introducing the simulation details, we demonstrate how to calculate certain observables using AMEP and briefly discuss the results. The code examples demonstrate the workflow of AMEP and serve as a guide for using AMEP. Further observables that are available in AMEP but which are not discussed in this section are exemplarily shown in Fig. 11.

A. Brownian dynamics simulations of active Brownian particles

As a first detailed example, we analyze particle-based simulation data obtained with the active Brownian particle (ABP) model as introduced in Section II as Eqs. (1) and (2). The repulsive interaction is modeled by the Weeks-Chandler-Anderson (WCA) potential $u(r_{ji}) = 4\epsilon[(\sigma/r_{ji})^{12} - (\sigma/r_{ji})^6] + \epsilon$, where $r_{ji} = |\vec{r}_j - \vec{r}_i|$ and $u = 0$ for $r_{ji}/\sigma \geq 2^{1/6}$ [175]. For the simulations here, we have chosen $l_p = 100\sigma$, $\epsilon/k_B T_b = 1.0$, and for simplicity, $\gamma_t = \gamma_r/\sigma^2$ unless otherwise stated (note that in experiments of active granulates, the Stokes-Einstein relation does not apply [176]). Here, $D_t = k_B T_b/\gamma_t$ and $D_r = k_B T_b/\gamma_r$ are the translational and rotational diffusion coefficients, respectively. We define the Péclet number as $Pe = v_0/\sqrt{2D_t D_r}$, which quantifies the strength of self-propulsion relative to diffusive motion. Note that all simulations are done in the overdamped regime, i.e., we choose a small mass $m/(\gamma_t \tau_p) = 5 \times 10^{-5}$. Since it has been found in previous works that the influence of the moment of inertia I on the simulation results is rather unimportant [72], it is held constant at $I/(\gamma_r \tau_p) = 0.33$ unless otherwise stated. All simulations are done within a two-dimensional quadratic box of length L with periodic boundary conditions and up to $N = 1.28 \times 10^6$ particles with a time step of $\Delta t/\tau_p = 10^{-5}$ – 10^{-6} using LAMMPS [173]. We choose $Pe = 70.7$ and a packing fraction of $\varphi = 0.5$ with $\varphi = N\pi\sigma^2/(4L^2)$ and start each simulation from uniformly distributed particle positions unless otherwise stated.

AMEP can load the common LAMMPS plain text format in which LAMMPS stores one snapshot of the simulation per text file named as `dump*.txt` for example, where the `*` is a placeholder for the current time step. These files are formatted as follows:

```
ITEM: TIMESTEP
20000
ITEM: NUMBER OF ATOMS
```

```
1280000
ITEM: BOX BOUNDS pp pp pp
0.0000000000000000e+00 1.5000000000000000e+03
0.0000000000000000e+00 1.5000000000000000e+03
-5.0000000000000000e-01 5.0000000000000000e-01
ITEM: ATOMS id type x y z fx fy mux muy radius mass
1 1 26.206 44.939 0 95.5607 9.87064 0.99913 0.04168 0.5 0.00005
2 1 45.187 24.985 0 -94.141 -33.726 -0.9414 -0.3373 0.5 0.00005
3 1 53.126 32.953 0 -86.024 12.4595 -0.9831 0.18303 0.5 0.00005
...
```

Here, `id` denotes a unique identifier for each particle, `type` denotes the particle type, `x,y,z` denote the position of each particle, `fx, fy` denote the forces acting on each particle, `mux, muy` are the components of the orientation vector \hat{p} , `radius` denotes the radius $\sigma/2$ of each particle, and `mass` their mass m . Note that `z` is zero for all particles because the simulation is done in two spatial dimensions. An exemplary dataset is available at <https://github.com/ameproject/amep/tree/main/examples>. AMEP reads all data from each text file and converts it into the `h5amep` format. Each item from the `ATOMS` section in the LAMMPS text file can then be accessed with the `.data()` method of the corresponding `BaseFrame` object, e.g., the force in x direction of frame 5 can be returned as NumPy array by calling

```
1 import amep
2 traj = amep.load.traj(
3     "/path/to/data",
4     mode = "lammps"
5 )
6 fx = traj[5].data("fx")
```

For many standard quantities such as coordinates, forces, or velocities, AMEP provides further commands exemplarily shown below:³

```
7 coords = traj[5].coords()
8 forces = traj[5].forces()
9 mu = traj[5].data("mux", "muy")
```

B. Motility-induced phase separation

For large enough packing fraction and large enough Pe , ABPs can phase separate into a dense and a dilute phase. This phenomenon is well-known as motility-induced phase separation (MIPS) [38, 43, 61–67, 72, 177] and can be understood as follows: If two ABPs collide, they can block each other due to their effective self-propulsion force. The collision can be resolved if the ABPs reorient their self-propulsion direction due to rotational diffusion and the self-propulsion direction of one ABP deviates from the other. Small clusters can form if more ABPs collide with the two ABPs blocking each other. Roughly, if now the mean time τ_c between collisions is smaller than the mean time τ_p a particle randomly reorients its self-propulsion direction, small clusters tend to grow, which finally results in a phase separation where an active gas coexists with a dense liquid [38, 40, 48, 178]. This process is exemplarily visualized by

³ See online documentation at <https://ameproject.de> for further details.

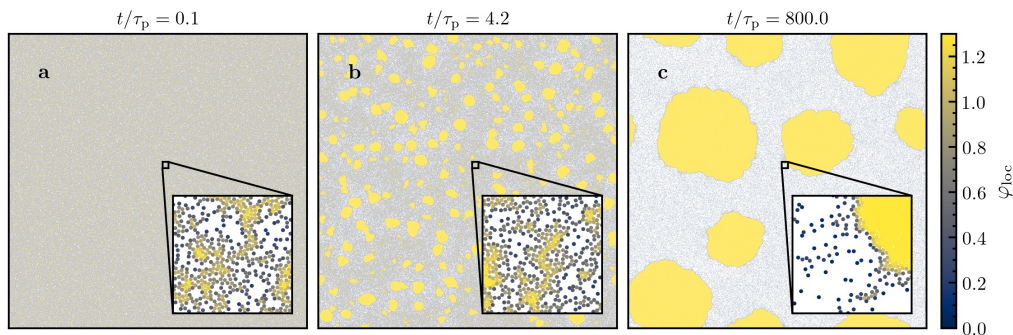


Figure 3. **Plotting snapshots with `amep.plot.particles`:** a–c Snapshots of ABPs undergoing MIPS starting from a uniform distribution for three different times as given in the key. The particles are colored with respect to their local area fraction φ_{loc} as obtained from a Voronoi tessellation calculated using `amep.order.voronoi_density` (see Subsection IV C for further details). The insets show the indicated extract of the simulation box and have been plotted using `amep.plot.add_inset`. Parameters: $m/(\gamma_t\tau_p) = 5 \times 10^{-5}$, $I/(\gamma_t\tau_p) = 0.33$, $N = 1.28 \times 10^6$, $\varphi = 0.5$, $\text{Pe} = 70.7$.

the snapshots shown in Fig. 3, which have been created using the `amep.plot.particles` function. In the following, we will mainly focus on the analysis of the simulation visualized in Fig. 3.

C. Voronoi diagrams and local order

Whether a simulation undergoes MIPS can be quantified by calculating the distribution of the local density or local area fraction, which is unimodal in the uniform regime and becomes bimodal in the MIPS regime [43, 47, 61, 179]. AMEP provides multiple functions to calculate the local density or area fraction: `amep.order.local_number_density`, `amep.order.local_mass_density`, and `amep.order.local_packing_fraction` determine the local number density, mass density, and area/volume fraction, respectively, from averages over circles of radius R , which can be written as $\varphi_{\text{loc}}(\vec{r}_i) = \sum_{j=1}^N \sigma_j^2 \text{H}(R - |\vec{r}_i - \vec{r}_j|) / (4R^2)$ in case of the local area fraction. Here, H is the Heaviside step function and σ_j is the diameter of particle j . Alternatively, `amep.order.voronoi_density` calculates the local mass density, number density, or area/volume fraction based on a Voronoi tessellation. Here, we will use the latter for calculating the distribution of (i) the local area fraction and (ii) the number of next neighbors.

The Voronoi diagram serves as a method for modeling the structures of materials across various disciplines, including crystallography, ecology, astronomy, epidemiology, geophysics, computer graphics, and more [180–184]. In essence, when given a set of points in the plane, the Voronoi diagram divides the plane based on the nearest neighbor rule, associating each point with the region of the plane closest to it. The mathematical definition extends to N -dimensions, often referred to as Voronoi tessellation [185, 186]. For a set of finite points $P = \{p_1, p_2, \dots, p_n\}$ in a subspace ζ in the Euclidean space, the Voronoi cell is formed through the division of the plane into regions, where each region encompasses

all points that are closer to each p_i . Points equidistant from at least two points in set P are not part of the Voronoi cell. Instead, they constitute the Voronoi edges. The compilation of all Voronoi cells forms the Voronoi tessellation associated with ζ .

The Voronoi tessellation is included in the `order` module of AMEP as function `amep.order.voronoi`. It calculates the Voronoi diagram for a given set of particle coordinates using the `scipy.spatial.Voronoi` class of the SciPy package [168]. Here, we use the Voronoi tessellation to calculate the number of next neighbors and the local area fraction. Let us first calculate the Voronoi diagram of the last frame (`traj[-1]`) via

```

1 import amep
2 # load the simulation data
3 traj = amep.load.traj(
4     "/path/to/data",
5     mode = "lammps"
6 )
7 # calculate the Voronoi diagram
8 vor, ids = amep.order.voronoi(
9     traj[-1].coords(),
10    traj[-1].box,
11    pbc = True
12 )

```

The obtained Voronoi diagram is demonstrated in Fig. 4a for the simulation snapshot shown in Fig. 3c. It can be easily visualized using `amep.plot.voronoi`. Next, we calculate the number of next neighbors from the Voronoi diagram and its distribution via

```

13 # number of next neighbors for each particle
14 nnn, -, -, -, - = amep.order.next_neighbors(
15    traj[-1].coords(),
16    traj[-1].box,
17    vor = vor,
18    ids = ids,
19    pbc = True
20 )
21 # distribution of the number of next neighbors
22 nndist, bins = amep.statistics.distribution(
23    nnn
24 )

```

As we can see in Fig. 4b, the distribution of the number of next neighbors attains its highest point at $N_{\text{nn}} = 6$. This observation indicates the existence of a hexagonal structure within the dense phase, as we will discuss in more

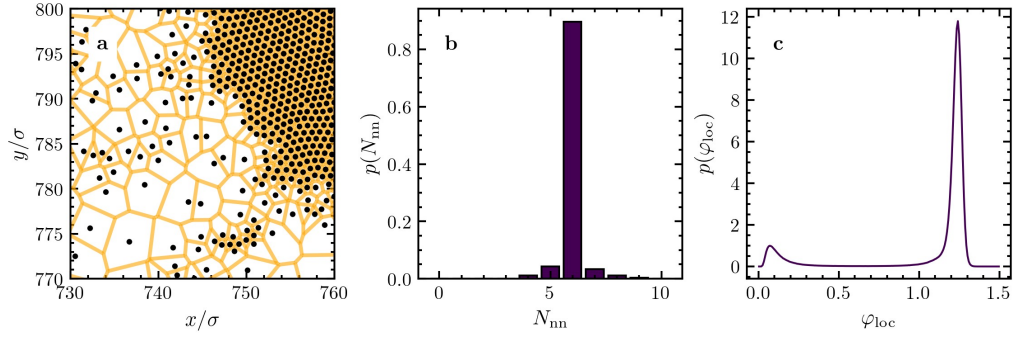


Figure 4. **Analyzing local order with the `amep.order` and `amep.evaluate` modules:** **a** Same extract of the simulation box as shown in the inset of Fig. 3c now with the corresponding Voronoi diagram obtained from `amep.order.voronoi` and plotted with `amep.plot.voronoi`. The black circles denote the particle positions, the orange lines the border of each Voronoi cell. **b** Distribution of the number of next neighbors obtained from the Voronoi diagram using `amep.order.next_neighbors` and `amep.statistics.distribution`. **c** Distribution of the local area fraction obtained from the areas of the Voronoi cells using `amep.evaluate.LDdist`. The results in panels b and c are averaged over five independent ensembles as exemplarily demonstrated in the code examples below. Parameters are the same as in Fig. 3.

detail below. Finally, we calculate the local area fraction using the Voronoi areas and evaluate its distribution:

```

25 # local area fraction of each particle
26 ld = amep.order.voronoi.density(
27     traj[-1].coords(),
28     traj[-1].box,
29     radius = traj[-1].radius(),
30     mode = "packing",
31     vor = vor,
32     ids = ids
33 )
34 # distribution of the local area fraction
35 lddist, bins = amep.statistics.distribution(
36     ld
37 )

```

If one would like to calculate the distribution of the local area fraction averaged over several frames of a trajectory, i.e., using a time average, one can simply create an `amep.evaluate.LDdist` object which is directly performing the time average and allows us to store the results in an HDF5 file. Additionally, multiple results can be stored in the same HDF5 file using AMEP's database feature: As an example, we calculate the distribution of the local area fraction for five independent simulation runs (ensembles) stored in directories `/path/to/data/do00-` `/path/to/data/do04` and store them together in one HDF5 file `ld.h5`:

```

1 import amep
2 # load all trajectories
3 trjs = [
4     amep.load.traj(
5         f"/path/to/data/do{i:02}",
6         mode = "lammers"
7     ) for i in range(5)
8 ]
9 for i, traj in enumerate(trjs):
10     # distribution of the local area fraction
11     ld = amep.evaluate.LDdist(
12         traj,
13         nav = traj.nframes,
14         use_voronoi = True,
15         mode = "packing"
16     )
17     # set name under which the data
18     # is stored in the HDF5 file
19     ld.name = f"do{i:02}"
20
21     # save all in file ld.h5

```

```
ld.save("ld.h5", database = True)
```

Now, we can calculate the ensemble average:

```

23 # load the analysis results
24 lds = amep.load.evaluation(
25     "ld.h5", database = True
26 )
27 # ensemble average
28 ensavg = 0.0
29 for i in range(5):
30     ensavg += lds[f"do{i:02}"].avg/5

```

The ensemble-averaged result is shown in Fig. 4c. As expected, the distribution of the local area fraction shows two peaks indicating that the system is phase-separated into a dense and a dilute phase. Note that the high-density peak is located at $\varphi_{loc} > 1.0$ due to the softness of the particles.

D. Hexagonal order

In the last paragraph, we saw that on average, each particle has six next neighbors, indicating that a hexagonal order dominates the local order of the particles. To quantify the local order in more detail, we calculate the hexagonal order parameter

$$\psi_6(\vec{r}_i) = \frac{1}{6} \sum_{j=1}^6 \exp\{i6\theta_{ij}\} \quad (6)$$

of each particle, where the sum goes over the six nearest neighbors of particle i and θ_{ij} is the angle between the connection line from \vec{r}_i to \vec{r}_j and the x axis [43, 187, 188]. In two spatial dimensions, the particles within the dense phase typically show local hexagonal order while they are disordered in the dilute phase. Therefore, the distribution of ψ_6 can also be used to assess whether a system is phase separated similarly to the local area fraction [43, 148, 188, 189]. Calculating the distribution of the hexagonal order parameter can be easily done using AMEP's evaluate module:

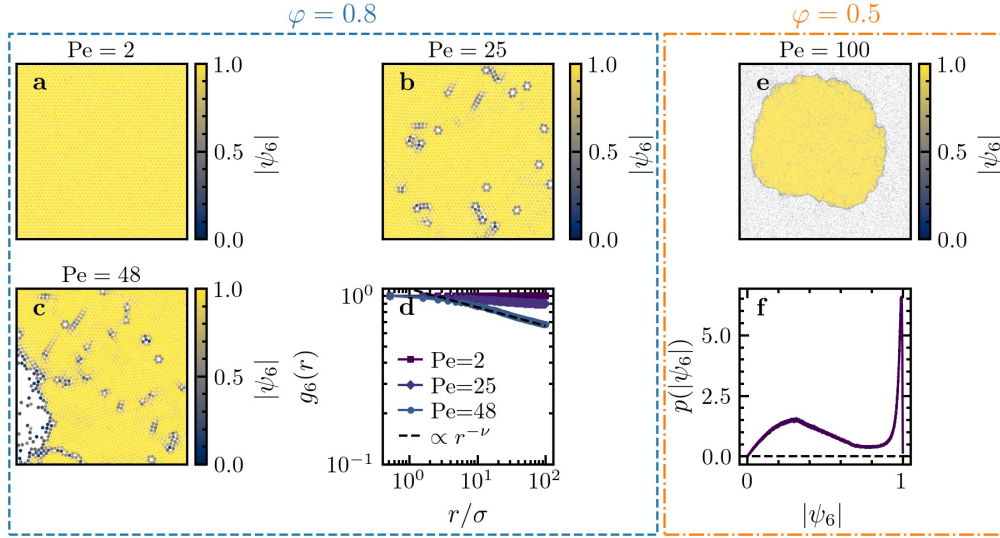


Figure 5. **Analyzing the hexagonal order using the `amep.order`, `amep.spatialcor`, and `amep.evaluate` modules:** **a–c** Extracts from the simulation box of an ABP system at high area fraction $\varphi = 0.8$ for $Pe = 2, 25, 48$, respectively. The particles are colored with respect to their hexagonal order parameter defined in Eq. (6) and calculated with `amep.order.psi.k`. Here, the simulations started from a hexagonal crystal as initial condition. **d** Spatial correlation function $g_6(r)$ as defined in Eq. (7) for the three snapshots shown in panels a–c averaged over three independent ensembles and over time in the steady state using `amep.evaluate.HexOrderCor`. The black dashed line shows an algebraic decay of the form $r^{-\nu}$ with exponent $\nu = 0.11$ as a guide for the eye. **e** Snapshot of one cluster of the simulation shown in Fig. 3c with $Pe = 70.7$ and $\varphi = 0.5$. Again, the particles are colored with respect to their hexagonal order parameter. **f** Distribution of the hexagonal order parameter corresponding to the snapshot shown in panel e calculated with `amep.evaluate.Psi6dist` and averaged over five independent ensembles. Parameters: $I/(\gamma_r\tau_p) = 5 \times 10^{-6}$, $N = 100\,000$, $\varphi = 0.8$, and $\epsilon/(k_B T_b) = 10$ (a–d), and (e–f) as in Fig. 3.

```

1 import amep
2 # load the simulation data
3 traj = amep.load.traj(
4     "/path/to/data",
5     mode = "lammps"
6 )
7 # psi6 distribution (all frames)
8 p6dist = amep.evaluate.Psi6dist(
9     traj,
10    nav = traj.nframes
11 )
12 # save results in HDF5 file
13 p6dist.save("p6dist.h5")
14
15 # plot the result of the last frame
16 fig, ax = amep.plot.new()
17 ax.plot(
18     p6dist.psi6,
19     p6dist.frames[-1,0]
20 )
21 fig.savefig("p6dist.png")

```

The result is demonstrated in Fig. 5f, where we have averaged over five independent ensembles. The broad peak at small values corresponds to the dilute phase while the sharp peak at $|\psi_6| = 1$ corresponds to the hexagonally packed dense phase as shown in Fig. 5e. It is also common to analyze the spatial range of the hexagonal order to check whether there exists a short-range or (quasi) long-range hexagonal order like in a crystal. To this end, one can calculate the spatial correlation function of the hexagonal order parameter

$$g_6(r) = \frac{\langle \psi_6^*(\vec{r}_i) \psi_6(\vec{r}_j) \rangle}{\langle |\psi_6(\vec{r}_i)|^2 \rangle} \quad (7)$$

with $r = |\vec{r}_i - \vec{r}_j|$ [43, 188]. Here, we calculate $g_6(r)$ for ABP simulations with $\epsilon/(k_B T_b) = 10$, $N = 100\,000$ particles, and at $\varphi = 0.8$ starting from a hexagonal lattice instead of a uniform distribution and average over multiple frames in the steady state:

```

1 import amep
2 # load simulation data
3 traj = amep.load.traj(
4     "/path/to/data",
5     mode = "lammps"
6 )
7 # calculate g6
8 g6 = amep.evaluate.HexOrderCor(
9     traj,
10    nav = traj.nframes,
11    njobs = 16,
12    rmax = 100.0,
13    skip = 0.5
14 )
15 # save results in an HDF5 file
16 g6.save(
17     "g6.h5"
18 )
19 # plot average
20 fig, ax = amep.plot.new()
21 ax.plot(
22     g6.r,
23     g6.avg
24 )
25 fig.savefig("g6.png")

```

Since this calculation is computationally expensive, we speed it up using parallelization by specifying the number of jobs that should run in parallel with the `njobs` keyword. Additionally, we give a maximum distance up to which the correlation function should be calculated and we skip

the first 50% of the trajectory to ensure that only the second half of the trajectory, which is in the steady state, is used for the calculation. The result is shown in Fig. 5d together with the corresponding snapshots in Fig. 5a–c for three different Pe . In accordance to Ref. [43], we observe a constant g_6 at small Pe and an algebraic decay of the form $r^{-\nu}$ with exponent ν at higher Pe .

E. Structure factor and coarsening

To further probe the order of an active system, one can exploit the radial distribution function $g(r)$, which we have exemplarily calculated in Section II using `amep.evaluate.RDF`. From an experimental viewpoint, it is easier to obtain the structure factor $S(\vec{q}, t)$, which is defined as [190]

$$S(\vec{q}, t) = \frac{1}{N} \left\langle \sum_{i=1}^N \sum_{j=1}^N \exp \{i\vec{q} \cdot [\vec{r}_i(t) - \vec{r}_j(t)]\} \right\rangle. \quad (8)$$

Here, \vec{q} represents the wave vector, $\vec{r}_i(t)$ and $\vec{r}_j(t)$ denote the positions of particles i and j at time t , respectively, and N is the total number of particles. For isotropic systems, the structure factor only depends on the magnitude $q = |\vec{q}|$ of the wave vector. It gives information about the density response to an external perturbation of wave length $2\pi/q$ and can be probed experimentally via scattering experiments. Note that $S(\vec{q}, t)$ is directly related to $g(\vec{r}, t)$ via Fourier transform. However, in practice, it is often preferable to calculate $S(\vec{q}, t)$ directly to achieve good numerical results in the low q regime. Within AMEP, $S(\vec{q}, t)$ can be directly calculated with `amep.evaluate.SF2d` and the isotropic structure factor $S(q, t)$ with $q = |\vec{q}|$ (i.e., $S(\vec{q}, t)$ averaged over the direction of \vec{q}) with `amep.evaluate.SFiso`. Here, we use $S(q, t)$ to analyze the coarsening process of the clusters forming when the ABPs undergo MIPS. To this end, we deduce a characteristic length scale $L(t)$ based on the first moment of $S(q, t)$ given by [84, 89, 144, 191, 192]

$$L(t) = \frac{\int_{2\pi/L}^{q_{\text{cut}}} S(q, t) dq}{\int_{2\pi/L}^{q_{\text{cut}}} q S(q, t) dq}, \quad (9)$$

where L is the length of the simulation box. We set the upper limit $q_{\text{cut}}\sigma = 0.3$, i.e., we only consider length scales larger than $2\pi/q_{\text{cut}} \approx 21\sigma$. Notably, under suitable conditions, overdamped ABPs undergoing MIPS exhibit an effective mapping onto a suitable equilibrium system at coarse-grained scales, as established in the literature [66]. This mapping explains why the coarsening dynamics follows the universal law $L(t) \sim t^{1/3}$ – a characteristic scaling behavior observed in equilibrium systems.

To visually elucidate this process, we present instances of $S(q, t)$ at distinct times $t/\tau_p = 0.1, 4.2, 800.0$ (Fig. 6a) corresponding to the snapshots shown in Fig. 3. These results can be obtained using the following code example:

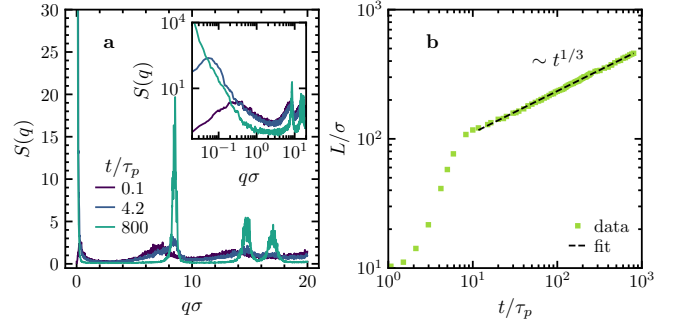


Figure 6. **Structure factor from `amep.evaluate.SFiso` and corresponding domain length from `amep.utils.domain_length`:** **a** Isotropic structure factor obtained from the three simulation snapshots shown in Fig. 3 using `amep.evaluate.SFiso`. The data is smoothed using a running average over seven points with the `amep.utils.runningmean` function. The inset shows the same data but with logarithmic axes. **b** Length scale $L(t)$ over time derived from the first moment of the structure factor as defined in Eq. (9) using the `amep.utils.domain_length` function. The data has been averaged over five independent ensembles and the black dashed line is a power-law fit of the form $L(t) = L_0 t^\alpha$ done with `amep.functions.Fit` resulting in an exponent $\alpha = 0.324 \pm 0.001$.

```

1 import amep
2 import numpy as np
3 # load simulation data
4 traj = amep.load.traj(
5     "/path/to/data",
6     mode = "lammps"
7 )
8 # calculate S(q)
9 sf = amep.evaluate.SFiso(
10     traj,
11     nav = traj.nframes
12 )
13 # plot S(q) of the last frame
14 fig, axs = amep.plot.new()
15 axs.plot(sf.q, sf.frames[-1][0])
16 fig.savefig("sf.pdf")

```

We can now subsequently compute $L(t)$ by using the `amep.utils.domain_length` function and fit a power-law of the form $L(t) = L_0 t^\alpha$ to it using `amep.functions.Fit`:

```

17 # calculate domain length
18 L = np.zeros(len(sf.frames))
19 for i, frame in enumerate(sf.frames):
20     length = amep.utils.domain_length(
21         frame[0], sf.q, qmax = 0.3
22     )
23     L[i] = length
24
25 # fit growth exponent
26 def f(x, L0 = 1, alpha = 1):
27     return L0*x**alpha
28 fit = amep.functions.Fit(f)
29 mask = sf.times > 10
30 fit.fit(sf.times[mask], L[mask])
31
32 # plot data and fit
33 fig, axs = amep.plot.new()
34 axs.plot(sf.times, L, label = "data")
35 axs.plot(
36     sf.times[mask],
37     fit.generate(sf.times[mask]),
38     marker = "", ls = "--",
39     label = "fit"

```

```

40 )
41 axs.legend()
42 fig.savefig("domain-length.pdf")

```

The result is illustrated in Fig. 6b and we obtain a growth exponent of $\alpha = 0.324 \pm 0.001$ in accordance with the literature [72, 89, 146].

F. Cluster analysis

Finally, we analyze the clustering of ABPs when undergoing MIPS by using AMEP's cluster module. For particle-based simulation data, we define a cluster as a collection of particles in which each particle has an interparticle distance smaller than r_{\max} to some other particle, where the cut-off distance r_{\max} can be chosen by the user. Particle i and j with position coordinates \vec{r}_i and \vec{r}_j , respectively, belong to the same cluster if $|\vec{r}_i - \vec{r}_j| \leq r_{\max}$. To find the distance between different particle pairs and identify the neighboring particle pairs that satisfy this distance criterion, we use the KDTree algorithm (`scipy.spatial.KDTree`) from the SciPy library [168, 193]. In the following, we will first show how to identify clusters using AMEP and afterwards analyze the coarsening of the clusters as well as their radius of gyration and fractal dimension.

Let us consider the last frame of a simulation showing MIPS (Fig. 3c). The clusters can be identified using the `amep.cluster.identify` function:

```

1 import amep
2 import numpy as np
3 # load simulation data
4 traj = amep.load.traj(
5     "/path/to/data",
6     mode = "lammps"
7 )
8 # get the last frame
9 frame = traj[-1]
10
11 # cluster detection
12 clusters, idx = amep.cluster.identify(
13     frame.coords(),
14     frame.box,
15     pbc = True,
16     rmax = 1.122
17 )

```

It takes the coordinates of all particles (`frame.coords()`) and the boundaries of the simulation box (`frame.box`) as an input and returns a list (`clusters`) of all clusters, sorted in descending order of their size, with each list element containing the indices of the particles belonging to the respective cluster. It also returns the array `idx` which stores the cluster indices assigned to each particle. The optional argument `pbc` is used to consider periodic boundary conditions and the cut-off distance `rmax` is set to the cut-off distance of the WCA potential (i.e., the contact distance). The algorithm works not only with simulation data of particles of the same size but can also identify clusters comprising particles of different sizes, which requires different values of the cut-off distance r_{\max} depending on the pair of particles. In the latter case, the user can provide the sizes of the particles (diameter) through the additional keyword `sizes` in `amep.cluster.identify`. In Fig.

7a, we show the same snapshot as in Fig. 3c, but with the particles of the eight largest clusters colored according to their cluster ids.

Based on the identified clusters, one can calculate various properties of the different clusters using the `cluster` module. One of them is the cluster size, defined as the number of particles within a cluster, the distribution of which often provides an insight into coexisting phases in a system [41, 194–200]. We can calculate the cluster sizes and masses by using the `amep.cluster.sizes` and `amep.cluster.masses` functions:

```

18 sizes = amep.cluster.sizes(
19     clusters
20 )
21 masses = amep.cluster.masses(
22     clusters, frame.data("mass")
23 )

```

Based on `sizes`, we can now calculate the cluster size distribution $p(s) = N_s / (\sum_s N_s)$, where N_s is the number of clusters with size s . Since we are interested in the coarsening behavior of the large clusters but their number is relatively small, it has been proven to be beneficial to analyze the weighted cluster size distribution

$$p_w(s) = \frac{sN_s}{\sum_s sN_s}, \quad (10)$$

where each cluster is weighted with its size s [201, 202]. Here, we use the `amep.statistics.distribution` function with logarithmic bins:

```

24 # weighted cluster size distribution
25 hist, bins = amep.statistics.distribution(
26     sizes, logbins = True,
27     nbins = 50, density = False
28 )
29 hist = hist*bins/np.sum(hist*bins)
30
31 # plot result
32 fig, axs = amep.plot.new()
33 axs.bar(
34     bins, hist, width = 0.2*bins
35 )
36 axs.loglog()
37 fig.savefig("size-dist.pdf")

```

The result is shown in Fig. 7b and exhibits two distinct peaks at small and large cluster sizes suggesting that the system is phase separated into two distinct phases. Large clusters characterize the dense liquid-like phase whereas the dilute gas-like phase comprises smaller clusters [41, 201, 202].

The cluster sizes can also be used to study the average growth rate of the clusters, which is a commonly used measure of the coarsening kinetics of phases in soft matter and biophysics [62, 75, 89, 146]. Here, we use `amep.evaluate.ClusterGrowth` to calculate the weighted mean cluster size $\langle s \rangle_w$ and the mean cluster size $\langle s \rangle$ defined as

$$\langle s \rangle_w = \sum_s s p_w(s) = \frac{\sum_s s^2 N_s}{\sum_s s N_s} \quad (11)$$

$$\langle s \rangle = \sum_s s p(s) = \frac{\sum_s s N_s}{\sum_s N_s} \quad (12)$$

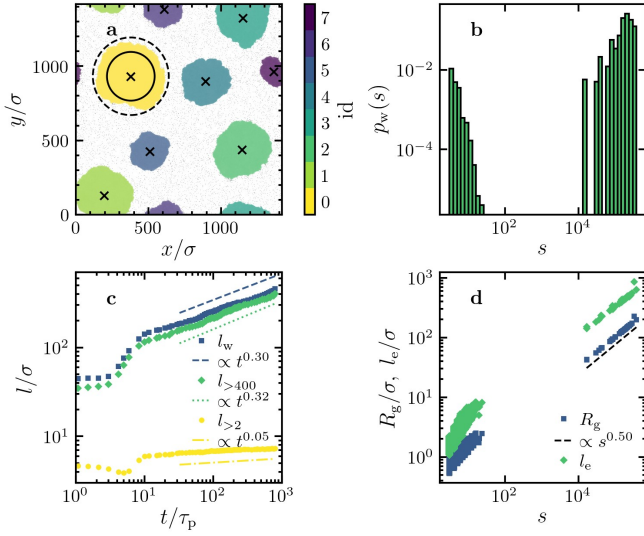


Figure 7. **Cluster analysis for particle-based simulation data with the `amep.cluster` and the `amep.evaluate` modules:** **a** Same snapshot as in Fig. 3c showing the eight largest clusters identified with the `amep.cluster.identify` function and colored with respect to their cluster index. The centers of mass of the clusters calculated with `amep.cluster.center_of_mass` are marked with black crosses. The black solid and dashed circles have radii equal to the radius of gyration and half the linear extension of the largest cluster (yellow) as obtained from Eqs. (13) and (14) using `amep.cluster.radius_of_gyration` and `amep.cluster.linear_extension`, respectively. **b** Weighted cluster size distribution as defined in Eq. (10) corresponding to the snapshot in panel a as obtained from `amep.evaluate.ClusterSizeDist` averaged over five independent ensembles. **c** Cluster length $l/\sigma = \sqrt{\langle s \rangle}$ calculated from the weighted mean cluster size $\langle s \rangle_w$ [Eq. (11)] and mean cluster sizes $\langle s \rangle_{>400}$ and $\langle s \rangle_{>2}$ [Eq. 12] averaged over all clusters larger than 400 and 2 particles, respectively, calculated using `amep.evaluate.ClusterGrowth` as function of time. The data has been averaged over five independent ensembles. The dashed, dotted, and dash-dotted lines are fits to $l(t) = l(0)t^\beta$ done with `amep.functions.Fit`. **d** Radius of gyration R_g and linear extension l_e as function of the cluster size s for the simulation shown in panel a. A fit to $R_g(s) \propto s^{1/d_f}$ results in a fractal dimension of $d_f = 1.99 \pm 0.03$.

over time (Fig. 7c). Similar to the domain length $L(t)$ obtained from the structure factor above, we will deduce a growth exponent from the growing mean cluster sizes. Note that for $L(t)$, we only considered $q\sigma < q_{\max}\sigma = 0.3$, i.e., length scales larger than $l_{\min} = 2\pi/q_{\max} \approx 21\sigma$, which resulted in a growth exponent of $\alpha \approx 1/3$ (where $L(t) \propto t^\alpha$). Since the cluster size measures the number of particles within a cluster, which is proportional to the area of the cluster, we can define a cluster length as $l/\sigma = \sqrt{\langle s \rangle}$ that is expected to also scale as $l \propto t^{1/3}$. However, this holds true only if we either disregard very small clusters that do not grow over time or assign greater importance to larger clusters by calculating the weighted mean cluster size. Therefore, additionally to the weighted mean cluster size, we also compute the

mean cluster size considering all the clusters (i.e., having at least two particles) and only the large clusters with at least 400 particles (in accordance to $l_{\min} \approx 21\sigma$ used for the calculation of $L(t)$).

```

38 # mean cluster size (>2)
39 mean.2 = amep.evaluate.ClusterGrowth(
40     traj,
41     mode = "mean",
42     min.size = 2
43 )
44 # mean cluster size (>400)
45 mean.400 = amep.evaluate.ClusterGrowth(
46     traj,
47     mode = "mean",
48     min.size = 400
49 )
50 # weighted mean cluster size
51 weighted.mean = amep.evaluate.ClusterGrowth(
52     traj,
53     mode = "weighted mean"
54 )

```

We now use `amep.functions.Fit` to obtain the growth exponent from $l(t) \propto t^\beta$ (here, exemplarily done for the weighted mean in the logarithmic domain):

```

55 # define fit function
56 def f(l, beta = 1.0, l0 = 1.0):
57     return np.log(l0) + beta*l
58
59 # create fit object
60 fit = amep.functions.Fit(f)
61
62 # fit function to data at large times
63 # in logarithmic domain
64 mask = weighted.mean.times > 3e1
65 fit.fit(
66     np.log(weighted.mean.times[mask]),
67     np.log(weighted.mean.frames[mask])/2
68 )
69 print(fit.results)
70
71 # plot data and fit
72 fig, axs = amep.plot.new()
73 axs.plot(
74     weighted.mean.times,
75     np.sqrt(weighted.mean.frames)
76 )
77 axs.plot(
78     weighted.mean.times[mask],
79     np.exp(fit.generate(
80         np.log(weighted.mean.times[mask])
81     ))
82 )
83 axs.loglog()
84 fig.savefig("cluster-growth.pdf")

```

```

{'beta': (0.297, 0.004),
 'l0': (64.6, 1.1)}

```

The results are demonstrated in Fig. 7c. Consistent with the established $\propto t^{1/3}$ growth of the characteristic domain length $L(t)$ of such ABP clusters [89], we obtain an exponent $\beta \approx 1/3$ for the cluster length calculated from the weighted mean and the mean over all clusters that are larger than 400 particles (Fig. 7c). For the mean over all clusters larger than two particles, the growth rate is significantly smaller because very small clusters do not grow.

To demonstrate the versatility of the cluster module, we present two additional calculable quantities using AMEP: the radius of gyration R_g and the linear extension l_e of the clusters. For a cluster composed of s particles of masses $m_i, i = 1, 2, \dots, s$, located at fixed distances d_i

from the cluster's center of mass, the radius of gyration is defined as [194, 203]

$$R_g = \sqrt{\frac{\sum_{i=1}^s m_i d_i^2}{\sum_{i=1}^s m_i}}. \quad (13)$$

The linear extension (also known as the end-to-end length) of a cluster is defined as the maximal distance between two particles in the cluster, i.e.,

$$l_e = \max_{\{i,j\}} |\vec{r}_i - \vec{r}_j|, \quad (14)$$

with \vec{r}_i denoting the position vector of the i -th particle and $i, j = 1, 2, \dots, s$ [194, 204]. The mean linear extension along with the mean size of the largest cluster is commonly used as an order parameter to characterize isotropic percolation phase transitions in different systems [194, 204, 205]. On the other hand, the dependence of the radius of gyration on the cluster size s (or mass) allows us to understand the (possibly fractal [206]) geometry of the clusters and calculate their fractal dimension d_f according to the relation $R_g \propto s^{1/d_f}$ [194, 206–213]. With AMEP, we can calculate such cluster properties easily by using its `cluster` module (here exemplarily done for the largest cluster):

```

85 # ids of particles in largest cluster
86 ids = clusters[0]
87
88 # center of mass
89 com = amep.cluster.center_of_mass(
90     frame.coords()[ids],
91     frame.box,
92     frame.data("mass")[ids],
93     pbc = True
94 )
95 # geometric center
96 gmc = amep.cluster.geometric_center(
97     frame.coords()[ids],
98     frame.box,
99     pbc = True
100 )
101 # radius of gyration
102 rg = amep.cluster.radius_of_gyration(
103     frame.coords()[ids],
104     frame.box,
105     frame.data("mass")[ids],
106     pbc = True
107 )
108 # linear extension
109 le = amep.cluster.linear_extension(
110     frame.coords()[ids],
111     frame.box,
112     frame.data("mass")[ids],
113     pbc = True
114 )

```

To handle periodic boundary conditions, AMEP uses the method proposed in Ref. [214]. The radius of gyration and the linear extension of the largest cluster are visualized in Fig. 7a. Additionally, we plotted R_g and l_e as function of the cluster size s in Fig. 7d to obtain the fractal dimension using `amep.functions.Fit` to fit the function $R_g(s) \propto s^{1/d_f}$. We obtain $d_f = 1.99 \pm 0.03$, i.e., essentially the same as the spatial dimension of the system, which is expected here since the clusters are compact.

V. ANALYZING CONTINUUM SIMULATION DATA WITH AMEP

Let us now discuss some examples on how to analyze continuum simulation data with AMEP. To this end, we will use numerical solutions of the active model B+, which is a corresponding continuum model for active Brownian particles. We will first introduce the model and afterwards demonstrate and discuss certain observables and minimal code examples using AMEP.

A. Active model B+

The active model B+ (AMB+) describes a system of active Brownian particles featuring a generic self-propulsion mechanism that can lead to interesting collective phenomena. It models the time evolution of the scalar field $\phi = (2\rho - \rho_H - \rho_L)/(\rho_H - \rho_L)$, where ρ_H and ρ_L denote the particle number density at the low-density and the high-density critical point, respectively [58, 144]. The active model B+ is given by [82]

$$\frac{\partial \phi}{\partial t} = -\nabla \cdot \left[-M \nabla \left(\frac{\delta \mathcal{F}}{\delta \phi} + \lambda |\nabla \phi|^2 \right) + \zeta M (\nabla^2 \phi) \nabla \phi + \sqrt{2k_B T M} \vec{\Lambda} \right], \quad (15)$$

$$\mathcal{F}[\phi] = \int d^3r \left[\frac{a}{2} \phi^2 + \frac{b}{4} \phi^4 + \frac{K}{2} |\nabla \phi|^2 \right]. \quad (16)$$

Here, the free-energy functional \mathcal{F} is approximated up to the order ϕ^4 and up to square-gradient terms, and $\vec{\Lambda}(\vec{r}, t)$ denotes Gaussian white noise with zero mean and unit variance. The mobility is denoted by M , the temperature is given by $k_B T$ with Boltzmann constant k_B , and a, b, K, ζ, λ are free parameters of the model. Here, we use $a = -0.25$, $b = 0.25$, $K = 1.0$, $\zeta = 1.0$, $\lambda = -0.5$, $k_B T = 0.2$, and $M = 1.0$ corresponding to a parameter regime showing phase separation [82]. We start from a uniform initial condition with $\phi_0 = -0.4$ disturbed with weak fluctuations. Here, we used an in-house finite volume solver written in C++ to numerically integrate Eq. (15) using a grid of 256×256 grid points with a grid spacing of $\Delta x = \Delta y = 1.0$ and time step $\Delta t = 0.001$. All simulations run for 10^8 time steps. To load the resulting data with AMEP, the data has to be stored in a certain data format as discussed in Subsection V E and as exemplified in the exemplary dataset which can be downloaded from <https://github.com/amepproject/amep/tree/main/examples>.

B. Motility-induced phase separation

Similar to the particle-based simulations of ABPs, the AMB+ also undergoes MIPS in a certain parameter regime [82]. Whether the system is phase separated can

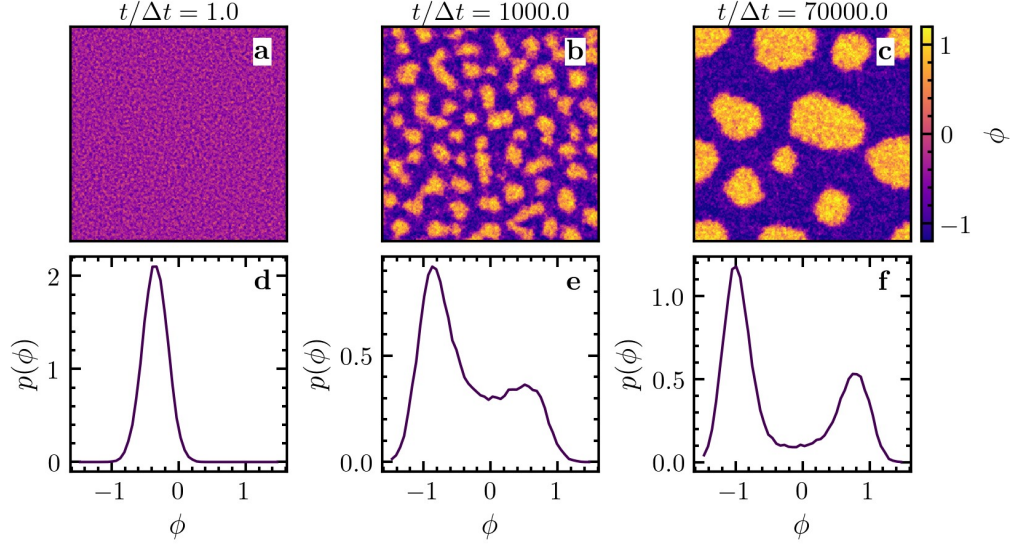


Figure 8. **Plotting snapshots with `amep.plot.field` and density distributions using `amep.evaluate.LDdist`: a–c** Snapshots of numerical solutions of the active model B+ as given in Eq. (15) plotted with `amep.plot.field` at three different times given in the key. **d–f** Corresponding density distributions calculated with `amep.evaluate.LDdist`.

again be determined by evaluating the local density distribution. In case of continuum data, one can simply calculate the distribution of the density at each grid point, as done by the `amep.evaluate.LDdist` class:

```

1 import amep
2 # load the data
3 traj = amep.load.traj(
4     "/path/to/data",
5     mode = "field"
6 )
7 # local density distribution of each frame
8 lddist = amep.evaluate.LDdist(
9     traj,
10    nav = traj.nframes,
11    xmin = -1.5,
12    xmax = 1.5,
13    ftype = "phi"
14 )
15 # save results in HDF5 file
16 lddist.save("lddist.h5")
17
18 # plot for the last frame
19 fig, axs = amep.plot.new()
20 axs.plot(lddist.ld, lddist.frames[-1,0])
21 axs.set_xlabel(r"$\phi_{\text{loc}}$")
22 axs.set_ylabel(r"$p(\phi_{\text{loc}})$")
23 fig.savefig("lddist.pdf")

```

The results are demonstrated in Fig. 8 at different times together with the corresponding snapshots. While the distribution is unimodal at the beginning of the simulations (which start with a uniform distribution), it becomes bimodal at long times showing that the system phase separates into a dense and a dilute phase by forming dense clusters that coexist with a surrounding gas-like phase.

C. Coarsening processes

Let us now analyze the coarsening behavior of the clusters based on the isotropic structure factor. For a continuum field, the (two-dimensional) structure factor can directly be calculated from the numerical Fourier transform of the scalar field ϕ as [144, 190, 215]

$$S(\vec{q}, t) = \langle \phi(\vec{q}, t) \phi(-\vec{q}, t) \rangle = \langle |\phi(\vec{q}, t)|^2 \rangle \quad (17)$$

using the `amep.continuum.sf2d` function. Here, $\phi(\vec{q}, t)$ is the spatial Fourier transform of $\phi(\vec{r}, t)$. To obtain the isotropic structure factor, the resulting two-dimensional structure factor must be averaged over the direction of \vec{q} , i.e., (using polar coordinates)

$$S(q, t) = \frac{1}{2\pi} \int_0^{2\pi} d\varphi S((q \cos(\varphi), q \sin(\varphi)), t) \quad (18)$$

which can be done in AMEP with the `amep.utils.sq.from_sf2d` function:

```

1 import amep
2 import numpy as np
3 # load data
4 traj = amep.load.traj(
5     "/path/to/data",
6     mode = "field"
7 )
8 # get last frame
9 frame = traj[-1]
10
11 # 2d structure factor
12 sf2d, qx, qy = amep.continuum.sf2d(
13     frame.data("phi"),
14     *frame.grid
15 )
16 # isotropic structure factor
17 sfiso, q = amep.utils.sq.from_sf2d(
18     sf2d, qx, qy
19 )

```


AMEP's evaluate module allows to calculate the isotropic structure factor directly from the traj object and also performs a time average:

```

20 # isotropic structure factor
21 # for all frames (time average)
22 sf = amep.evaluate.SFiso(
23     traj,
24     nav = traj.nframes,
25     ftype = "phi"
26 )

```

Here, we can specify which field of the given trajectory should be used via ftype. From the structure factor, we can then again calculate the domain length as defined in Eq. (9) via

```

27 # domain length over time
28 L = np.zeros(traj.nframes)
29 for i, f in enumerate(sf.frames):
30     L[i] = amep.utils.domain.length(
31         f[0], f[1]
32     )

```

Note that we do not specify q_{\max} here because we integrate over all q up to its largest possible value $q_{\max} = \pi/\Delta x$ given by the grid spacing Δx . The results are demonstrated in Fig. 9, which shows three exemplary curves of the structure factor at three different times and the domain length over time. From the domain length, we extract the growth exponent by fitting a power law to the domain length at long times in the logarithmic domain:

```

33 # define fit function
34 def f(t, L0 = 1.0, alpha = 1.0):
35     return np.log(L0) + alpha*t
36 # create fit object
37 fit = amep.functions.Fit(f)
38
39 # fit at large times
40 mask = traj.times > 1e1
41 fit.fit(
42     np.log(traj.times[mask]),
43     np.log(L[mask])
44 )
45 print(fit.results)

```

```

{'L0': (4.168, 0.085),
 'alpha': (0.2702, 0.0029)}

```

Interestingly, for our continuum simulations of the active model B+, we obtain $\alpha \approx 0.27$, which is smaller than the value $\alpha \approx 1/3$ as obtained in our particle-based simulations. Such subdiffusive scaling has been obtained in previous studies of active field theories as well and is typically expected to be an intermediate scaling regime that leads to a $t^{1/3}$ scaling at longer times [84, 89, 144].

D. Cluster analysis

Next, we will analyze the clusters forming at late times in more detail by performing a similar cluster analysis as done in Subsection IV F. For the continuum data, a cluster is defined as a connected region of similar and higher density than the surroundings. AMEP provides two algorithms to detect clusters in continuum data (i.e., discretized density fields). The standard algorithm is dividing up pixels according to their values relative to a

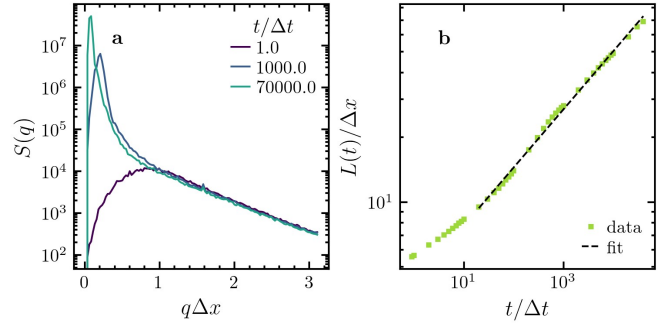


Figure 9. **Structure factor from `amep.evaluate.SFiso` and corresponding domain length from `amep.utils.domain.length` for continuum simulation data:** **a** Isotropic structure factor obtained from the three simulation snapshots of the active model B+ shown in Fig. 8 calculated with `amep.evaluate.SFiso`. Note that the upper limit for the wave vector q is given by the resolution of the discretized grid, i.e., $q_{\max} = \pi/\Delta x$. **b** Length scale $L(t)$ as obtained from Eq. (9) using the `amep.utils.domain.length` function. The data has been averaged over five independent ensembles and the black dashed line is a power-law fit of the form $L(t) = L_0 t^\alpha$ done with `amep.functions.Fit` and resulting in a growth exponent of $\alpha = 0.270 \pm 0.003$.

threshold value, i.e., for a scalar continuum field ϕ , a zero is assigned to all pixels with $\phi \leq a_{\text{thres}}(\phi_{\max} - \phi_{\min})$ and a one to all pixels with $\phi > a_{\text{thres}}(\phi_{\max} - \phi_{\min})$. Here, $a_{\text{thres}} \in [0, 1]$ denotes the relative threshold and ϕ_{\min} , ϕ_{\max} are the minimum and maximum values of the continuum field. On the resulting two-valued image, all connected regions are then labeled as a cluster using `skimage.measure.label` [168, 216, 217]. Within AMEP, this algorithm is called `"threshold"`. An alternative way for cluster detection is the watershed algorithm [218]. It is more stable against slowly varying background fields but needs more fine-tuning of parameters to work. Therefore, the watershed algorithm is not the first choice for detecting clusters over time, i.e., for multiple frames of a trajectory, because the parameters may need to be adjusted for each frame individually. In AMEP, the `skimage.segmentation.watershed` function is used for the `"watershed"` cluster detection [168].

Clusters within a continuum field can be identified with AMEP using the `amep.continuum.identify_clusters` function. In the following example, we detect the clusters in the last frame of a continuum simulation using the `"threshold"` method:

```

1 import amep
2 # load data
3 traj = amep.load.traj(
4     "path/to/data",
5     mode = "field"
6 )
7 # get the last frame
8 frame = traj[-1]
9
10 # identify clusters
11 ids, labels = \
12     amep.continuum.identify_clusters(
13         frame.data("phi"),
14         pbc = True,

```

```

15     threshold = 0.1,
16     method = "threshold"
17 )

```

Here, `frame.data("phi")` returns an array of values of field "phi" at each point of the underlying discretized grid, the `pbk` keyword can be set to `True` to apply periodic boundary conditions, and `threshold` specifies the relative threshold a_{thres} . The keyword `method` chooses between the "threshold" or "watershed" method. The `amep.continuum.identify_clusters` function assigns a unique identifier to each detected cluster returned as NumPy array (`ids` in the example above), and it returns an array of the same shape as the underlying discretized grid denoting which grid point belongs to which cluster (labels in the example above). The result is exemplarily visualized in Fig. 10a.

As a next step, the `amep.continuum.cluster_properties` function can be used to calculate certain properties of the detected clusters such as their sizes, masses, centers, or radii of gyration:

```

18 s, gmc, com, rg, le, gt, it = \
19 amep.continuum.cluster_properties(
20     frame.data("phi"),
21     *frame.grid,
22     ids,
23     labels,
24     pbk = True
25 )

```

where `s`, `gmc`, `com`, `rg`, `le`, `gt`, `it` denote the size, geometric center, center of mass, radius of gyration, linear extension, gyration tensor, and inertia tensor of each cluster, respectively. Here, the size of cluster i within a field ϕ is defined as the integral over its area A_i , i.e., $s_i = \int_{A_i} d^2r \phi(\vec{r})$. All other cluster properties are calculated with the same methods as used for the particle-based simulation data by treating each grid point (i, j) as a particle at position \vec{r}_{ij} with "mass" $\phi(\vec{r}_{ij})$. The radius of gyration and the linear extension of the largest cluster are visualized in Fig. 10a.

Similarly to the cluster analysis for particle-based data, we can now calculate the weighted cluster-size distribution, the growth exponents, and the fractal dimension of the clusters exploiting AMEP's `evaluate` module. Let us first calculate the weighted cluster-size distribution as defined in Eq. (10):

```

26 # weighted cluster size distribution
27 cd = amep.evaluate.ClusterSizeDist(
28     traj,
29     nav = traj.nframes,
30     ftype = "phi",
31     method = "threshold",
32     threshold = 0.1,
33     use_density = False,
34     nbins = 50,
35     logbins = True,
36     xmin = 1e0,
37     xmax = 1e4
38 )

```

Here, the keyword `use_density` allows to specify whether the integrated density s_i (`use_density = True`) as defined above or area A_i (`use_density = False`) should be used as size of cluster i . Furthermore, we have used the threshold method and logarithmic bins and the result is shown in Fig. 10b. Next, we analyze the cluster growth by calculating the average cluster size over time using the

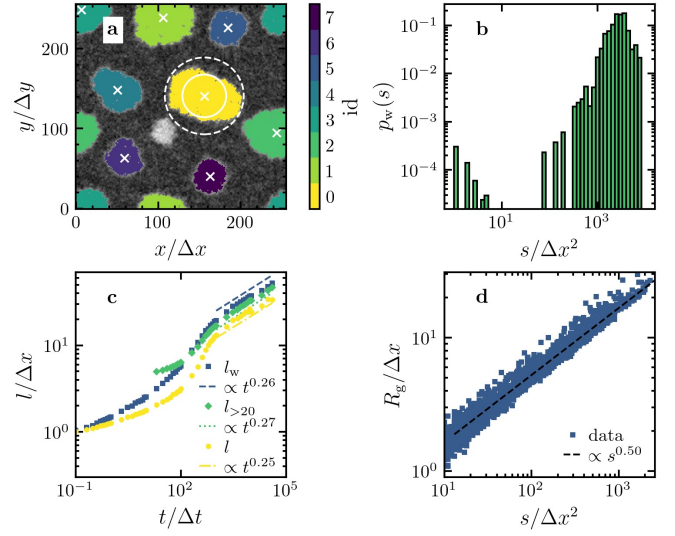


Figure 10. **Cluster analysis for continuum simulation data with the `amep.continuum` and the `amep.evaluate` modules.** **a** Same snapshot as in Fig. 8c showing the eight largest clusters identified with the `amep.continuum.identify_clusters` function and colored with respect to their cluster index. The centers of mass of the clusters calculated with `amep.continuum.cluster_properties` are marked with white crosses. The white solid and dashed circles have radii equal to the radius of gyration and half the linear extension of the largest cluster (yellow) as obtained from Eqs. (13) and (14), respectively, using `amep.continuum.cluster_properties`. **b** Weighted cluster size distribution as defined in Eq. (10) corresponding to the snapshot in panel a as obtained from `amep.evaluate.ClusterSizeDist` averaged over five independent ensembles. **c** Cluster length $l = \sqrt{\langle s \rangle}$ obtained from the weighted mean cluster size $\langle s \rangle_w$ [Eq. (11)] and mean cluster sizes $\langle s \rangle$ [Eq. 12] and $\langle s \rangle_{>20}$ averaged over all clusters and over all clusters larger than an area of $20\Delta x^2$, respectively, calculated using `amep.evaluate.ClusterGrowth` as function of time. The data has been averaged over five independent ensembles. The dashed, dotted, and dash-dotted lines are fits to $l(t) = l(0)t^\beta$ done with `amep.functions.Fit`. **d** Radius of gyration R_g as function of the cluster size s for five independent simulations as exemplarily shown in panel a. A fit to $R_g(s) \propto s^{1/d_f}$ results in a fractal dimension of $d_f = 1.99 \pm 0.01$.

weighted mean and mean as defined in Eqs. (11) and (12), respectively:

```

39 # mean cluster sizes
40 mean = amep.evaluate.ClusterGrowth(
41     traj,
42     ftype = "phi",
43     method = "threshold",
44     mode = "mean",
45     threshold = 0.1,
46     use_density = False
47 )
48 # mean cluster size over all clusters
49 # with size larger than 20
50 mean_20 = amep.evaluate.ClusterGrowth(
51     traj,
52     ftype = "phi",
53     method = "threshold",

```

```

54 mode = "mean",
55 threshold = 0.1,
56 use_density = False,
57 min_size = 20
58 )
59 # weighted mean cluster size
60 amep.functions.ClusterGrowth(
61     traj,
62     ftype = "phi",
63     method = "threshold",
64     mode = "weighted mean",
65     threshold = 0.1,
66     use_density = False
67 )

```

Again, we define the cluster length as $l = \sqrt{\langle s \rangle}$ and use `amep.functions.Fit` to obtain the growth exponent from $l(t) \propto t^\beta$ as already demonstrated in Subsection IV F. Consistent with the growth exponent $\alpha \approx 0.27$ obtained from the domain length $L(t)$ (see Subsection V C), we obtain $\beta \approx 0.26$ (Fig. 10c). Additionally, we plotted the radius of gyration R_g as function of the cluster size s in Fig. 10d to obtain the fractal dimension using `amep.functions.Fit` to fit the function $R_g(s) \propto s^{1/d_f}$. We obtain $d_f = 1.99 \pm 0.01$, i.e., the same as the spatial dimension of the system, which is expected here since the clusters are compact.

E. Continuum data format

Continuum simulation data as analyzed within this work has to be stored in a specific format such that it can be loaded with AMEP. In the following, we briefly introduce the basic format requirements. In AMEP, field data is internally stored using the `h5amep` file format, similar to the particle-based simulation data. Converting field data to an AMEP dataset is done by use of a reader class (`amep.reader.ContinuumReader`). This data reader expects the following format: The standard file structure for field data is inspired by the LAMMPS dump file format, i.e., all relevant data is stored in one base directory which contains (i) a file named `grid.txt` and (ii) multiple files named `field_<index>.txt`. The former is of the form

```

BOX:
<X_min> <X_max>
<Y_min> <Y_max>
<Z_min> <Z_max>
SHAPE:
<nx> <ny> <nz>
COORDINATES: X Y Z
<X_0> <Y_0> <Z_0>
<X_1> <Y_0> <Z_0>
...
<X_N> <Y_0> <Z_0>
<X_0> <Y_1> <Z_0>
<X_1> <Y_1> <Z_0>
...

```

and contains all information about the simulation box and the underlying discrete grid. The values in the

BOX category define the borders of the simulation box, which is assumed to be rectangular, the SHAPE category contains the shape of the grid, and COORDINATES contains the coordinates of all grid points. If the data is based on an evenly spaced rectangular grid and the grid points are given in rising order, the SHAPE category tells AMEP in what kind of multidimensional array the data should be cast for representation. The files named `field_<index>.txt` contain all data that varies in time. The index should rise in time and could be chosen as the number of timesteps for example. The data files should be of the following form:

```

TIMESTEP:
<Simulation timestep>
TIME:
<Physical time>
DATA: <name 0> <name 1> <name 2> <name 3>
<field 0 0> <field 1 0> <field 2 0> <field 3 0>
<field 0 1> <field 1 1> <field 2 1> <field 3 1>
<field 0 2> <field 1 2> <field 2 2> <field 3 2>
...

```

Here, the names describe the scalar field written to the column beneath, e.g., density. The columns are then filled by the values of the respective field at each grid point in the same order as in `grid.txt`. The columns can be separated by spaces, tabs, commas, semicolons, colons, or a vertical bar. The TIMESTEP category contains the number of timesteps corresponding to the contained data and the TIME category the corresponding (physical) time. If you have data of this type in the directory `/path/to/data`, it can be loaded with AMEP via

```

1 field_trajectory = amep.load.traj(
2     "/path/to/data",
3     mode = "field",
4     delimiter = " ",
5     dumps = "field_*.txt",
6     reload = True
7 )

```

The `mode` keyword tells AMEP to expect field data, `delimiter` specifies the delimiter used for the columns in the data files, `dumps` takes a regular expression that matches the name format of the variable data files, and the keyword `reload` tells AMEP whether to look for an existing `h5amep` file and use it if it exists or to create a new one from the raw data. This should be used when your base data has changed between analysis runs. An exemplary dataset can be downloaded from <https://github.com/ameproject/amep/tree/main/examples>.

VI. CONCLUSION

AMEP is a powerful Python library for analyzing simulation data of active matter systems. It provides a unified framework for handling both particle-based and continuum simulation data and combines it with an easy-to-learn Python API. With AMEP, one can quickly analyze and plot simulation results and develop new analysis

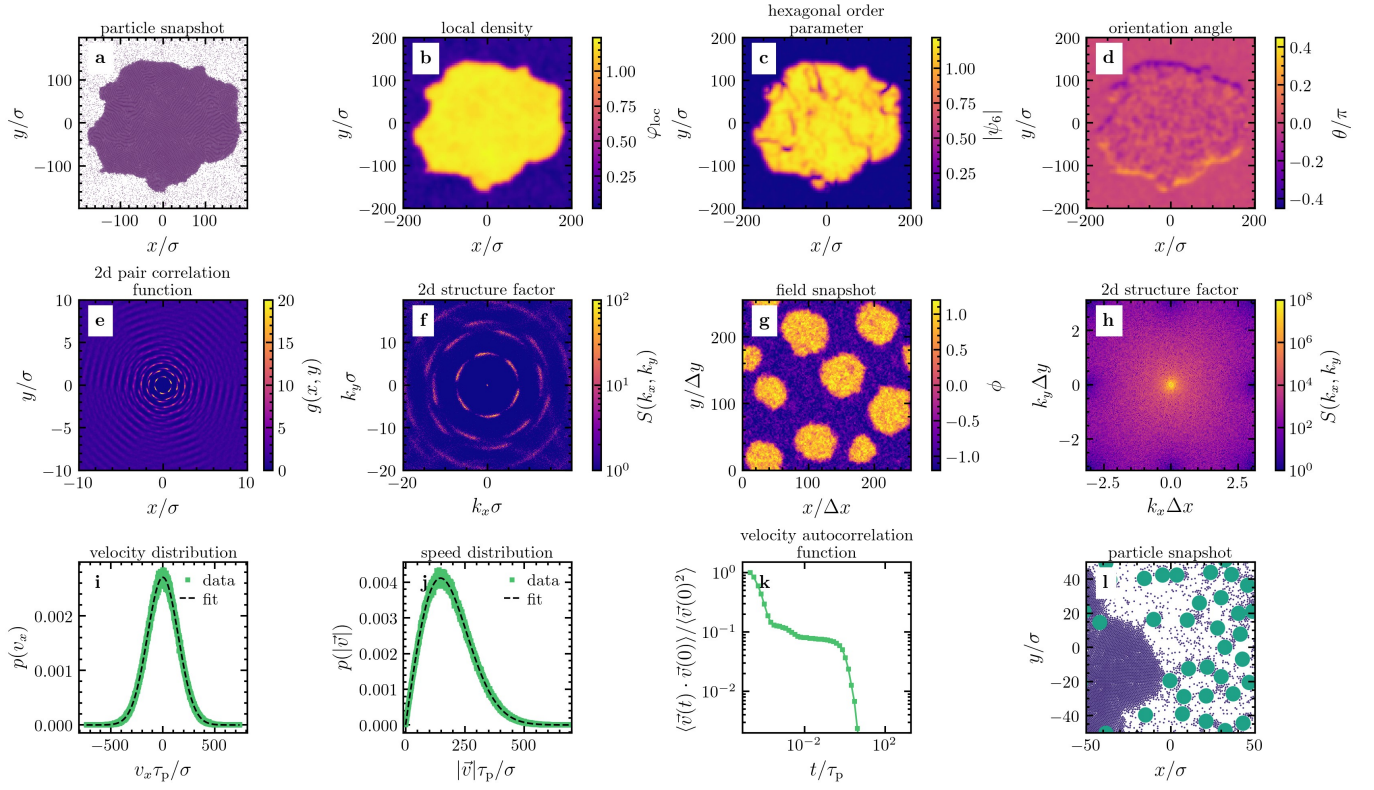


Figure 11. **Further observables calculated with AMEP:** **a** Snapshot of MIPS plotted with `amep.plot.particles`. **b–d** Corresponding coarse-grained local density φ_{loc} , hexagonal order parameter ψ_6 [Eq. (6)], and orientation angle θ , respectively, calculated with `amep.continuum.gkde`. **e** Two-dimensional pair correlation function of the snapshot shown in panel **a** calculated with `amep.evaluate.PCF2d`. **f** Two-dimensional structure factor of the snapshot shown in panel **a** calculated with `amep.evaluate.SF2d`. **g** Snapshot of MIPS in the active model B+ plotted with `amep.plot.field`. **h** Two-dimensional structure factor of the field shown in panel **g** calculated with `amep.evaluate.SF2d`. **i,j** Distribution of the velocity v_x in x direction and the magnitude $|\vec{v}|$ from a particle-based simulation in two spatial dimensions calculated with `amep.evaluate.VelDist`. The black dashed lines are fits obtained with `amep.functions.NormalizedGaussian` and `amep.functions.MaxwellBoltzmann`, respectively. **k** Velocity autocorrelation function calculated with `amep.evaluate.VACF`. **l** Snapshot of a simulation with particles of different sizes plotted with `amep.plot.particles`.

methods utilizing AMEP’s features and its seamless integrability to powerful scientific Python libraries through NumPy arrays. While its collection of analysis methods is primarily targeted at the active matter community, AMEP’s general design allows to apply AMEP to almost any particle-based or continuum simulation data as obtained from classical molecular-dynamics and Brownian-dynamics simulations, or any kind of numerical solutions of partial differential equations.

We have exemplarily shown the potential of AMEP by analyzing particle-based systems of more than 10^6 particles and continuum simulations with up to 10^5 grid points as typically used in active matter research. AMEP enables the analysis of a broader class of simulation data compared to most other analysis libraries. Such simulation data comprises “dry” particle-based models such as the active Brownian particle model and its various relatives, “wet” models that explicitly model surrounding fluids including particles that are coupled to flow fields, and continuum models such as the active model B+,

the Keller-Segel model, or the Cahn-Hilliard model. Applied to such models, AMEP can provide essential insights, e.g., into phase separation, pattern formation, and critical phenomena in active matter systems. In addition to the presented observables, many more observables will be included in the future, for instance, entropy production using the method introduced in Ref. [125], finite-size scaling analysis, and cluster tracking. We would like to encourage the active matter community to contribute to this open-source project in order to complement it with future analysis methods for particle-based and continuum simulation data.

CREDIT AUTHORSHIP CONTRIBUTION STATEMENT

Lukas Hecht: conceptualization, data curation, formal analysis, funding acquisition, investigation, methodology, project administration, software, validation, visu-

alization, writing (original draft and review & editing). **Kay-Robert Dormann:** formal analysis, methodology, software, visualization, writing (original draft and review & editing). **Kai Luca Spanheimer:** formal analysis, methodology, software, visualization, writing (original draft and review & editing). **Mahdieh Ebrahimi:** formal analysis, software, visualization, writing (original draft and review & editing). **Malte Cordts:** software. **Suwendu Mandal:** formal analysis, investigation, software, visualization, writing (original draft and review & editing). **Aritra K. Mukhopadhyay:** formal analysis, methodology, software, visualization, writing (original draft and review & editing). **Benno Liebchen:** conceptualization, funding acquisition, project administration, supervision, writing (review & editing).

DECLARATION OF COMPETING INTEREST

The authors declare that they have no known competing financial interests or personal relationships that

could have appeared to influence the work reported in this paper.

ACKNOWLEDGEMENTS

L.H. and B.L. gratefully acknowledge the computing time provided to them at the NHR Center NHR4CES at TU Darmstadt (project number p0020259). This is funded by the Federal Ministry of Education and Research, and the state governments participating on the basis of the resolutions of the GWK for national high performance computing at universities (www.nhr-verein.de/unsere-partner). L.H. gratefully acknowledges the support by the German Academic Scholarship Foundation (Studienstiftung des deutschen Volkes). A.K.M. and B.L. acknowledge financial support from the Deutsche Forschungsgemeinschaft (DFG, German Research Foundation) through project number 233630050 (TRR-146).

-
- [1] M. Karplus and J. A. McCammon, Molecular dynamics simulations of biomolecules, *Nat. Struct. Biol.* **9**, 646 (2002).
 - [2] I. Kumari, P. Sandhu, M. Ahmed, and Y. Akhter, Molecular Dynamics Simulations, Challenges and Opportunities: A Biologist's Perspective, *Curr. Protein Pept. Sci.* **18**, 1163 (2017).
 - [3] P. R. L. Markwick and J. A. McCammon, Studying functional dynamics in bio-molecules using accelerated molecular dynamics, *Phys. Chem. Chem. Phys.* **13**, 20053 (2011).
 - [4] S. Mogurampelly, O. Borodin, and V. Ganesan, Computer Simulations of Ion Transport in Polymer Electrolyte Membranes, *Annu. Rev. Chem. Biomol. Eng.* **7**, 349 (2016).
 - [5] N. Yao, X. Chen, Z.-H. Fu, and Q. Zhang, Applying Classical, Ab Initio, and Machine-Learning Molecular Dynamics Simulations to the Liquid Electrolyte for Rechargeable Batteries, *Chem. Rev.* **122**, 10970 (2022).
 - [6] J. B. Haskins, W. R. Bennett, J. J. Wu, D. M. Hernández, O. Borodin, J. D. Monk, C. W. Bauschlicher, and J. W. Lawson, Computational and Experimental Investigation of Li-Doped Ionic Liquid Electrolytes: [pyr14][TFSI], [pyr13][FSI], and [EMIM][BF₄], *J. Phys. Chem. B* **118**, 11295 (2014).
 - [7] M. R. Wilson, Progress in computer simulations of liquid crystals, *Int. Rev. Phys. Chem.* **24**, 421 (2005).
 - [8] Y. Huang, W. Wang, J. K. Whitmer, and R. Zhang, Structures, thermodynamics and dynamics of topological defects in Gay-Berne nematic liquid crystals, *Soft Matter* **19**, 483 (2023).
 - [9] G. Watanabe, A. Yamazaki, and J. Yoshida, The Missing Relationship between the Miscibility of Chiral Dopants and the Microscopic Dynamics of Solvent Liquid Crystals: A Molecular Dynamics Study, *Symmetry* **15**, 1092 (2023).
 - [10] R. Horstmann, L. Hecht, S. Kloth, and M. Vogel, Structural and Dynamical Properties of Liquids in Confinements: A Review of Molecular Dynamics Simulation Studies, *Langmuir* **38**, 6506 (2022).
 - [11] T. Pal, C. Beck, D. Lessnich, and M. Vogel, Effects of Silica Surfaces on the Structure and Dynamics of Room-Temperature Ionic Liquids: A Molecular Dynamics Simulation Study, *J. Phys. Chem. C* **122**, 624 (2018).
 - [12] S. Mandal, S. Lang, M. Gross, M. Oettel, D. Raabe, T. Franosch, and F. Varnik, Multiple reentrant glass transitions in confined hard-sphere glasses, *Nat. Commun.* **5**, 4435 (2014).
 - [13] S. Mandal and T. Franosch, Diverging Time Scale in the Dimensional Crossover for Liquids in Strong Confinement, *Phys. Rev. Lett.* **118**, 065901 (2017).
 - [14] F. Guarra and G. Colombo, Computational Methods in Immunology and Vaccinology: Design and Development of Antibodies and Immunogens, *J. Chem. Theory Comput.* **19**, 5315 (2023).
 - [15] S. Rafi, S. Yasmin, and R. Uddin, A molecular dynamic simulation approach: development of dengue virus vaccine by affinity improvement techniques, *J. Biomol. Struct. Dyn.* **40**, 61 (2022).
 - [16] A. Smith, X. Dong, and V. Raghavan, An Overview of Molecular Dynamics Simulation for Food Products and Processes, *Processes* **10**, 119 (2022).
 - [17] G. De Magistris and D. Marenduzzo, An introduction to the physics of active matter, *Physica A* **418**, 65 (2015).
 - [18] C. Bechinger, R. Di Leonardo, H. Löwen, C. Reichhardt, G. Volpe, and G. Volpe, Active Particles in Complex and Crowded Environments, *Rev. Mod. Phys.* **88**, 045006 (2016).
 - [19] J. Elgeti, R. G. Winkler, and G. Gompper, Physics of microswimmers—single particle motion and collective behavior: a review, *Rep. Prog. Phys.* **78**, 056601 (2015).

- [20] G. Liu, A. Patch, F. Bahar, D. Yllanes, R. D. Welch, M. C. Marchetti, S. Thutupalli, and J. W. Shaevitz, Self-Driven Phase Transitions Drive *Myxococcus xanthus* Fruiting Body Formation, *Phys. Rev. Lett.* **122**, 248102 (2019).
- [21] C. Wolgemuth, E. Hoiczyk, D. Kaiser, and G. Oster, How *Myxobacteria* Glide, *Curr. Biol.* **12**, 369 (2002).
- [22] S. Rafai, L. Jibuti, and P. Peyla, Effective Viscosity of Microswimmer Suspensions, *Phys. Rev. Lett.* **104**, 098102 (2010).
- [23] J. R. Howse, R. A. L. Jones, A. J. Ryan, T. Gough, R. Vafabakhsh, and R. Golestanian, Self-Motile Colloidal Particles: From Directed Propulsion to Random Walk, *Phys. Rev. Lett.* **99**, 048102 (2007).
- [24] B. Liebchen and H. Löwen, Synthetic Chemotaxis and Collective Behavior in Active Matter, *Acc. Chem. Res.* **51**, 2982 (2018).
- [25] L. Qiao, M.-J. Huang, and R. Kapral, Active motion of synthetic nanomotors in filament networks, *Phys. Rev. Res.* **2**, 033245 (2020).
- [26] C. Kurzthaler, Y. Zhao, N. Zhou, J. Schwarz-Linek, C. Devailly, J. Arlt, J.-D. Huang, W. C. Poon, T. Franosch, J. Tailleur, *et al.*, Characterization and Control of the Run-and-Tumble Dynamics of *Escherichia Coli*, *Phys. Rev. Lett.* **132**, 038302 (2024).
- [27] G. Ramos, M. L. Cordero, and R. Soto, Bacteria driving droplets, *Soft Matter* **16**, 1359 (2020).
- [28] C. Kurzthaler, C. Devailly, J. Arlt, T. Franosch, W. C. Poon, V. A. Martinez, and A. T. Brown, Probing the Spatiotemporal Dynamics of Catalytic Janus Particles with Single-Particle Tracking and Differential Dynamic Microscopy, *Phys. Rev. Lett.* **121**, 078001 (2018).
- [29] J. Grauer, H. Löwen, and B. Liebchen, Strategic spatiotemporal vaccine distribution increases the survival rate in an infectious disease like Covid-19, *Sci. Rep.* **10**, 21594 (2020).
- [30] A. Attanasi, A. Cavagna, L. Del Castello, I. Giardina, T. S. Grigera, A. Jelić, S. Melillo, L. Parisi, O. Pohl, E. Shen, *et al.*, Information transfer and behavioural inertia in starling flocks, *Nat. Phys.* **10**, 691 (2014).
- [31] D. Klotsa, As above, so below, and also in between: mesoscale active matter in fluids, *Soft Matter* **15**, 8946 (2019).
- [32] J. Buhl, D. J. T. Sumpter, I. D. Couzin, J. J. Hale, E. Despland, E. R. Miller, and S. J. Simpson, From Disorder to Order in Marching Locusts, *Science* **312**, 1402 (2006).
- [33] C. K. Hemelrijk and H. Hildenbrandt, Schools of fish and flocks of birds: their shape and internal structure by self-organization, *Interface Focus* **2**, 726 (2012).
- [34] M. Ballerini, N. Cabibbo, R. Candelier, A. Cavagna, E. Cisbani, I. Giardina, V. Lecomte, A. Orlandi, G. Parisi, A. Procaccini, *et al.*, Interaction ruling animal collective behavior depends on topological rather than metric distance: Evidence from a field study, *Proc. Natl. Acad. Sci.* **105**, 1232 (2008).
- [35] W. Bialek, A. Cavagna, I. Giardina, T. Mora, E. Silvestri, M. Viale, and A. M. Walczak, Statistical mechanics for natural flocks of birds, *Proc. Natl. Acad. Sci.* **109**, 4786 (2012).
- [36] J. L. Silverberg, M. Bierbaum, J. P. Sethna, and I. Cohen, Collective Motion of Humans in Mosh and Circle Pits at Heavy Metal Concerts, *Phys. Rev. Lett.* **110**, 228701 (2013).
- [37] N. Bain and D. Bartolo, Dynamic response and hydrodynamics of polarized crowds, *Science* **363**, 46 (2019).
- [38] M. E. Cates and J. Tailleur, Motility-Induced Phase Separation, *Annu. Rev. Condens. Matter Phys.* **6**, 219 (2015).
- [39] J. Barré, R. Chétrite, M. Muratori, and F. Peruani, Motility-Induced Phase Separation of Active Particles in the Presence of Velocity Alignment, *J. Stat. Phys.* **158**, 589 (2015).
- [40] G. Gonnella, D. Marenduzzo, A. Suma, and A. Tiribocchi, Motility-induced phase separation and coarsening in active matter, *Comptes Rendus Phys.* **16**, 316 (2015).
- [41] I. Buttinoni, J. Bialké, F. Kümmel, H. Löwen, C. Bechinger, and T. Speck, Dynamical Clustering and Phase Separation in Suspensions of Self-Propelled Colloidal Particles, *Phys. Rev. Lett.* **110**, 238301 (2013).
- [42] J. Blaschke, M. Maurer, K. Menon, A. Zöttl, and H. Stark, Phase separation and coexistence of hydrodynamically interacting microswimmers, *Soft Matter* **12**, 9821 (2016).
- [43] P. Digregorio, D. Levis, A. Suma, L. F. Cugliandolo, G. Gonnella, and I. Pagonabarraga, Full Phase Diagram of Active Brownian Disks: From Melting to Motility-Induced Phase Separation, *Phys. Rev. Lett.* **121**, 098003 (2018).
- [44] F. Bergmann, L. Rapp, and W. Zimmermann, Active phase separation: A universal approach, *Phys. Rev. E* **98**, 020603 (2018).
- [45] P. Dolai, A. Simha, and S. Mishra, Phase separation in binary mixtures of active and passive particles, *Soft Matter* **14**, 6137 (2018).
- [46] J. Zhang, R. Alert, J. Yan, N. S. Wingreen, and S. Granick, Active phase separation by turning towards regions of higher density, *Nat. Phys.* **17**, 961 (2021).
- [47] J. Su, H. Jiang, and Z. Hou, Inertia-induced nucleation-like motility-induced phase separation, *New J. Phys.* **23**, 013005 (2021).
- [48] F. D. C. Farrell, M. C. Marchetti, D. Marenduzzo, and J. Tailleur, Pattern Formation in Self-Propelled Particles with Density-Dependent Motility, *Phys. Rev. Lett.* **108**, 248101 (2012).
- [49] B. Liebchen, D. Marenduzzo, I. Pagonabarraga, and M. E. Cates, Clustering and Pattern Formation in Chemorepulsive Active Colloids, *Phys. Rev. Lett.* **115**, 258301 (2015).
- [50] B. Liebchen and D. Levis, Collective Behavior of Chiral Active Matter: Pattern Formation and Enhanced Flocking, *Phys. Rev. Lett.* **119**, 058002 (2017).
- [51] D. Saintillan and M. J. Shelley, Instabilities and Pattern Formation in Active Particle Suspensions: Kinetic Theory and Continuum Simulations, *Phys. Rev. Lett.* **100**, 178103 (2008).
- [52] A. P. Solon, J.-B. Caussin, D. Bartolo, H. Chaté, and J. Tailleur, Pattern formation in flocking models: A hydrodynamic description, *Phys. Rev. E* **92**, 062111 (2015).
- [53] M. F. Hagan and A. Baskaran, Emergent self-organization in active materials, *Curr. Opin. Cell Biol.* **38**, 74 (2016).
- [54] J. Palacci, B. Abécassis, C. Cottin-Bizonne, C. Ybert, and L. Bocquet, Colloidal Motility and Pattern Formation under Rectified Diffusiophoresis, *Phys. Rev. Lett.* **104**, 138302 (2010).

- [55] J. Toner and Y. Tu, Flocks, herds, and schools: A quantitative theory of flocking, *Phys. Rev. E* **58**, 4828 (1998).
- [56] D. Levis, I. Pagonabarraga, and B. Liebchen, Activity induced synchronization: Mutual flocking and chiral self-sorting, *Phys. Rev. Res.* **1**, 023026 (2019).
- [57] R. Chatterjee, N. Rana, R. A. Simha, P. Perlekar, and S. Ramaswamy, Inertia Drives a Flocking Phase Transition in Viscous Active Fluids, *Phys. Rev. X* **11**, 031063 (2021).
- [58] M. R. Shaebani, A. Wysocki, R. G. Winkler, G. Gompper, and H. Rieger, Computational models for active matter, *Nat. Rev. Phys.* **2**, 181 (2020).
- [59] L. Hecht, J. C. Ureña, and B. Liebchen, An Introduction to Modeling Approaches of Active Matter, arXiv:2102.13007 [cond-mat.soft] (2021).
- [60] P. Romanczuk, M. Bär, W. Ebeling, B. Lindner, and L. Schimansky-Geier, Active Brownian particles, *Eur. Phys. J. Spec. Top.* **202**, 1 (2012).
- [61] S. De Karmakar and R. Ganesh, Motility-induced phase separation of self-propelled soft inertial disks, *Soft Matter* **18**, 7301 (2022).
- [62] G. S. Redner, M. F. Hagan, and A. Baskaran, Structure and Dynamics of a Phase-Separating Active Colloidal Fluid, *Phys. Rev. Lett.* **110**, 055701 (2013).
- [63] J. Su, M. Feng, Y. Du, H. Jiang, and Z. Hou, Motility-induced phase separation is reentrant, *Commun. Phys.* **6**, 58 (2023).
- [64] G. S. Redner, C. G. Wagner, A. Baskaran, and M. F. Hagan, Classical Nucleation Theory Description of Active Colloid Assembly, *Phys. Rev. Lett.* **117**, 148002 (2016).
- [65] S. C. Takatori and J. F. Brady, Towards a thermodynamics of active matter, *Phys. Rev. E* **91**, 032117 (2015).
- [66] T. Speck, J. Bialké, A. M. Menzel, and H. Löwen, Effective Cahn-Hilliard Equation for the Phase Separation of Active Brownian Particles, *Phys. Rev. Lett.* **112**, 218304 (2014).
- [67] J. Tailleur and M. E. Cates, Statistical Mechanics of Interacting Run-and-Tumble Bacteria, *Phys. Rev. Lett.* **100**, 218103 (2008).
- [68] M. Rojas-Vega, P. de Castro, and R. Soto, Mixtures of self-propelled particles interacting with asymmetric obstacles, *Eur. Phys. J. E* **46**, 95 (2023).
- [69] Z. Ma and R. Ni, Dynamical clustering interrupts motility-induced phase separation in chiral active Brownian particles, *J. Chem. Phys.* **156**, 10.1063/5.0077389 (2022).
- [70] P. Nie, J. Chatteraj, A. Piscitelli, P. Doyle, R. Ni, and M. P. Ciamarra, Stability phase diagram of active Brownian particles, *Phys. Rev. Res.* **2**, 023010 (2020).
- [71] J. Yang, R. Ni, and M. P. Ciamarra, Interplay between jamming and motility-induced phase separation in persistent self-propelling particles, *Phys. Rev. E* **106**, L012601 (2022).
- [72] S. Mandal, B. Liebchen, and H. Löwen, Motility-Induced Temperature Difference in Coexisting Phases, *Phys. Rev. Lett.* **123**, 228001 (2019).
- [73] L. Hecht, S. Mandal, H. Löwen, and B. Liebchen, Active Refrigerators Powered by Inertia, *Phys. Rev. Lett.* **129**, 178001 (2022).
- [74] P. Digregorio, D. Levis, L. F. Cugliandolo, G. Gonnella, and I. Pagonabarraga, Unified analysis of topological defects in 2D systems of active and passive disks, *Soft Matter* **18**, 566 (2022).
- [75] C. B. Caporusso, L. F. Cugliandolo, P. Digregorio, G. Gonnella, D. Levis, and A. Suma, Dynamics of Motility-Induced Clusters: Coarsening beyond Ostwald Ripening, *Phys. Rev. Lett.* **131**, 068201 (2023).
- [76] S. Saw, L. Costigliola, and J. C. Dyre, Configurational temperature in active matter. I. Lines of invariant physics in the phase diagram of the Ornstein-Uhlenbeck model, *Phys. Rev. E* **107**, 024609 (2023).
- [77] A. K. Omar, K. Klymko, T. GrandPre, P. L. Geissler, and J. F. Brady, Tuning nonequilibrium phase transitions with inertia, *J. Chem. Phys.* **158**, 42 (2023).
- [78] A. R. Sprenger, L. Caprini, H. Löwen, and R. Wittmann, Dynamics of active particles with translational and rotational inertia, *J. Phys. Condens. Matter* **35**, 305101 (2023).
- [79] E. Schiltz-Rouse, H. Row, and S. A. Mallory, Kinetic temperature and pressure of an active Tonks gas, *Phys. Rev. E* **108**, 064601 (2023).
- [80] M. Sandoval, Free and enclosed inertial active gas, *Soft Matter* **19**, 6287 (2023).
- [81] P.-C. Chen, K. Kroy, F. Cichos, X. Wang, and V. Holubec, Active particles with delayed attractions form quaking crystallites $\langle \sup \rangle (a) \langle /sup \rangle$, *Europhys. Lett.* **142**, 67003 (2023).
- [82] E. Tjhung, C. Nardini, and M. E. Cates, Cluster Phases and Bubbly Phase Separation in Active Fluids: Reversal of the Ostwald Process, *Phys. Rev. X* **8**, 031080 (2018).
- [83] A. Tiribocchi, R. Wittkowski, D. Marenduzzo, and M. E. Cates, Active Model H: Scalar Active Matter in a Momentum-Conserving Fluid, *Phys. Rev. Lett.* **115**, 188302 (2015).
- [84] J. Stenhammar, A. Tiribocchi, R. J. Allen, D. Marenduzzo, and M. E. Cates, Continuum Theory of Phase Separation Kinetics for Active Brownian Particles, *Phys. Rev. Lett.* **111**, 145702 (2013).
- [85] S. Mishra, A. Baskaran, and M. C. Marchetti, Fluctuations and pattern formation in self-propelled particles, *Phys. Rev. E* **81**, 061916 (2010).
- [86] H. Zhao, A. Košmrlj, and S. S. Datta, Chemotactic Motility-Induced Phase Separation, *Phys. Rev. Lett.* **131**, 118301 (2023).
- [87] J. Berx, A. Bose, R. Golestanian, and B. Mahault, Reentrant condensation transition in a model of driven scalar active matter with diffusivity edge, *Europhys. Lett.* **142**, 67004 (2023).
- [88] E. Sesé-Sansa, G.-J. Liao, D. Levis, I. Pagonabarraga, and S. H. L. Klapp, Impact of dipole-dipole interactions on motility-induced phase separation, *Soft Matter* **18**, 5388 (2022).
- [89] J. Stenhammar, D. Marenduzzo, R. J. Allen, and M. E. Cates, Phase behaviour of active Brownian particles: the role of dimensionality, *Soft Matter* **10**, 1489 (2014).
- [90] A. M. Menzel, A. Saha, C. Hoell, and H. Löwen, Dynamical density functional theory for microswimmers, *J. Chem. Phys.* **144**, 024115 (2016).
- [91] C. Hoell, H. Löwen, and A. M. Menzel, Particle-scale statistical theory for hydrodynamically induced polar ordering in microswimmer suspensions, *J. Chem. Phys.* **149**, 10.1063/1.5048304 (2018).
- [92] C. Hoell, H. Löwen, and A. M. Menzel, Dynamical density functional theory for circle swimmers, *New J. Phys.* **19**, 10.1088/1367-2630/aa942e (2017).

- [93] R. Soto, M. Pinto, and R. Brito, Kinetic theory of motility induced phase separation for active Brownian particles, arXiv:2401.16260v1 [cond-mat.soft] (2024).
- [94] D. S. Dean, Langevin equation for the density of a system of interacting Langevin processes, *J. Phys. A: Math. Gen.* **29**, L613 (1996).
- [95] H. Risken, *The Fokker-Planck Equation*, Springer Series in Synergetics (Springer, Berlin, Heidelberg, 1984).
- [96] Y. Fily and M. C. Marchetti, Athermal Phase Separation of Self-Propelled Particles with No Alignment, *Phys. Rev. Lett.* **108**, 235702 (2012).
- [97] J. Grauer, H. Löwen, A. Be'er, and B. Liebchen, Swarm Hunting and Cluster Ejections in Chemically Communicating Active Mixtures, *Sci. Rep.* **10**, 5594 (2020).
- [98] X. Jiang, H. Jiang, and Z. Hou, Nonlinear chemical reaction induced abnormal pattern formation of chemotactic particles, *Soft Matter* **19**, 3946 (2023).
- [99] B. Liebchen, D. Marenduzzo, and M. E. Cates, Phoretic Interactions Generically Induce Dynamic Clusters and Wave Patterns in Active Colloids, *Phys. Rev. Lett.* **118**, 268001 (2017).
- [100] A. V. Zampetaki, B. Liebchen, A. V. Ivlev, and H. Löwen, Collective self-optimization of communicating active particles, *Proc. Natl. Acad. Sci.* **118**, 1 (2021).
- [101] F. Fadda, D. A. Matoz-Fernandez, R. van Roij, and S. Jabbari-Farouji, The interplay between chemophoretic interactions and crowding in active colloids, *Soft Matter* **19**, 2297 (2023).
- [102] A. Fischer, A. Chatterjee, and T. Speck, Aggregation and sedimentation of active Brownian particles at constant affinity, *J. Chem. Phys.* **150**, 10.1063/1.5081115 (2019).
- [103] S. Saha, R. Golestanian, and S. Ramaswamy, Clusters, asters, and collective oscillations in chemotactic colloids, *Phys. Rev. E* **89**, 062316 (2014).
- [104] O. Pohl and H. Stark, Dynamic Clustering and Chemotactic Collapse of Self-Phoretic Active Particles, *Phys. Rev. Lett.* **112**, 238303 (2014).
- [105] B. Liebchen and A. K. Mukhopadhyay, Interactions in active colloids, *J. Phys. Condens. Matter* **34**, 083002 (2022).
- [106] A. Zöttl and H. Stark, Modeling Active Colloids: From Active Brownian Particles to Hydrodynamic and Chemical Fields, *Annu. Rev. Condens. Matter Phys.* **14**, 109 (2023).
- [107] B. Liebchen and H. Löwen, Modeling Chemotaxis of Microswimmers: From Individual to Collective Behavior, in *Chem. Kinet.* (World Scientific, Singapore, 2019) p. 493.
- [108] E. F. Keller and L. A. Segel, Model for chemotaxis, *J. Theor. Biol.* **30**, 225 (1971).
- [109] A. R. Sprenger, C. Bair, and H. Löwen, Active Brownian motion with memory delay induced by a viscoelastic medium, *Phys. Rev. E* **105**, 044610 (2022).
- [110] G. H. P. Nguyen, R. Wittmann, and H. Löwen, Active Ornstein-Uhlenbeck model for self-propelled particles with inertia, *J. Phys. Condens. Matter* **34**, 035101 (2022).
- [111] E. A. Lisin, O. S. Vaulina, I. I. Lisina, and O. F. Petrov, Motion of a self-propelled particle with rotational inertia, *Phys. Chem. Chem. Phys.* **24**, 14150 (2022).
- [112] L. Caprini and U. M. B. Marconi, Inertial self-propelled particles, *J. Chem. Phys.* **154**, 024902 (2021).
- [113] J. Reichert and T. Voigtmann, Tracer dynamics in crowded active-particle suspensions, *Soft Matter* **17**, 10492 (2021).
- [114] M. Sandoval, Pressure and diffusion of active matter with inertia, *Phys. Rev. E* **101**, 012606 (2020).
- [115] D. Breoni, M. Schmiedeberg, and H. Löwen, Active Brownian and inertial particles in disordered environments: Short-time expansion of the mean-square displacement, *Phys. Rev. E* **102**, 062604 (2020).
- [116] E. Lemaitre, I. M. Sokolov, R. Metzler, and A. V. Chechkin, Non-Gaussian displacement distributions in models of heterogeneous active particle dynamics, *New J. Phys.* **25**, 013010 (2023).
- [117] T. Debnath, S. Nayak, P. Bag, D. Debnath, and P. K. Ghosh, Structure and diffusion of active-passive binary mixtures in a single-file, *J. Chem. Sci.* **135**, 38 (2023).
- [118] P. Nie, J. Chattoraj, A. Piscitelli, P. Doyle, R. Ni, and M. P. Ciamarra, Frictional active Brownian particles, *Phys. Rev. E* **102**, 032612 (2020).
- [119] H. Wang, F. H. Stillinger, and S. Torquato, Sensitivity of pair statistics on pair potentials in many-body systems, *J. Chem. Phys.* **153**, 124106 (2020).
- [120] E. Gavagnin, J. P. Owen, and C. A. Yates, Pair correlation functions for identifying spatial correlation in discrete domains, *Phys. Rev. E* **97**, 062104 (2018).
- [121] G. Szamel, E. Flenner, and L. Berthier, Glassy dynamics of athermal self-propelled particles: Computer simulations and a nonequilibrium microscopic theory, *Phys. Rev. E* **91**, 062304 (2015).
- [122] S. Bröker, M. te Vrugt, J. Jeggle, J. Stenhammar, and R. Wittkowski, Pair-distribution function of active Brownian spheres in three spatial dimensions: simulation results and analytical representation, *Soft Matter* **20**, 224 (2024).
- [123] D. Frydel, Entropy production of active particles formulated for underdamped dynamics, *Phys. Rev. E* **107**, 014604 (2023).
- [124] J. O'Byrne, Y. Kafri, J. Tailleur, and F. van Wijland, Time irreversibility in active matter, from micro to macro, *Nat. Rev. Phys.* **4**, 167 (2022).
- [125] S. Ro, B. Guo, A. Shih, T. V. Phan, R. H. Austin, D. Levine, P. M. Chaikin, and S. Martiniani, Model-Free Measurement of Local Entropy Production and Extractable Work in Active Matter, *Phys. Rev. Lett.* **129**, 220601 (2022).
- [126] T. GrandPre, K. Klymko, K. K. Mandadapu, and D. T. Limmer, Entropy production fluctuations encode collective behavior in active matter, *Phys. Rev. E* **103**, 012613 (2021).
- [127] É. Fodor and M. E. Cates, Active engines: Thermodynamics moves forward, *Europhys. Lett.* **134**, 10003 (2021).
- [128] D. Mandal, K. Klymko, and M. R. DeWeese, Entropy Production and Fluctuation Theorems for Active Matter, *Phys. Rev. Lett.* **119**, 258001 (2017).
- [129] S. De Karmakar and R. Ganesh, Phase transition and emergence of active temperature in an active Brownian system in underdamped background, *Phys. Rev. E* **101**, 032121 (2020).
- [130] U. M. B. Marconi, A. Puglisi, and C. Maggi, Heat, temperature and Clausius inequality in a model for active Brownian particles, *Sci. Rep.* **7**, 46496 (2017).

- [131] L. F. Cugliandolo, G. Gonnella, and I. Petrelli, Effective Temperature in Active Brownian Particles, *Fluct. Noise Lett.* **18**, 1940008 (2019).
- [132] Z. Zhang and R. Garcia-Millan, Entropy production of nonreciprocal interactions, *Phys. Rev. Res.* **5**, L022033 (2023).
- [133] L. Dabelow, S. Bo, and R. Eichhorn, How irreversible are steady-state trajectories of a trapped active particle?, *J. Stat. Mech. Theory Exp.* **2021**, 033216 (2021).
- [134] L. F. Cugliandolo, The effective temperature, *J. Phys. A Math. Theor.* **44**, 483001 (2011).
- [135] G. Szamel, Stochastic thermodynamics for self-propelled particles, *Phys. Rev. E* **100**, 050603(R) (2019).
- [136] T. Herpich, K. Shayanfar, and M. Esposito, Effective thermodynamics of two interacting underdamped Brownian particles, *Phys. Rev. E* **101**, 022116 (2020).
- [137] P. Gaspard and R. Kapral, Active Matter, Microreversibility, and Thermodynamics, *Research* **2020**, 1 (2020).
- [138] V. Venkatasubramanian, A. Sivaram, and L. Das, A unified theory of emergent equilibrium phenomena in active and passive matter, *Comput. Chem. Eng.* **164**, 107887 (2022).
- [139] S. S. Khali, F. Peruani, and D. Chaudhuri, When an active bath behaves as an equilibrium one, *Phys. Rev. E* **109**, 024120 (2024).
- [140] F. Dittrich, T. Speck, and P. Virnau, Critical behavior in active lattice models of motility-induced phase separation, *Eur. Phys. J. E* **44**, 53 (2021).
- [141] J. T. Siebert, F. Dittrich, F. Schmid, K. Binder, T. Speck, and P. Virnau, Critical behavior of active Brownian particles, *Phys. Rev. E* **98**, 030601(R) (2018).
- [142] N. Gnan and C. Maggi, Critical behavior of quorum-sensing active particles, *Soft Matter* **18**, 7654 (2022).
- [143] A. Sinha and D. Chaudhuri, How reciprocity impacts ordering and phase separation in active nematics?, *Soft Matter* **20**, 788 (2024).
- [144] R. Wittkowski, A. Tiribocchi, J. Stenhammar, R. J. Allen, D. Marenduzzo, and M. E. Cates, Scalar ϕ^4 field theory for active-particle phase separation, *Nat. Commun.* **5**, 4351 (2014).
- [145] X.-q. Shi, G. Fausti, H. Chaté, C. Nardini, and A. Solon, Self-Organized Critical Coexistence Phase in Repulsive Active Particles, *Phys. Rev. Lett.* **125**, 168001 (2020).
- [146] C. B. Caporusso, P. Digregorio, D. Levis, L. F. Cugliandolo, and G. Gonnella, Motility-Induced Microphase and Macrophase Separation in a Two-Dimensional Active Brownian Particle System, *Phys. Rev. Lett.* **125**, 178004 (2020).
- [147] M. N. van der Linden, L. C. Alexander, D. G. Aarts, and O. Dauchot, Interrupted Motility Induced Phase Separation in Aligning Active Colloids, *Phys. Rev. Lett.* **123**, 098001 (2019).
- [148] M. Paoluzzi, D. Levis, and I. Pagonabarraga, From motility-induced phase-separation to glassiness in dense active matter, *Commun. Phys.* **5**, 111 (2022).
- [149] L. Caprini, U. M. B. Marconi, C. Maggi, M. Paoluzzi, and A. Puglisi, Hidden velocity ordering in dense suspensions of self-propelled disks, *Phys. Rev. Res.* **2**, 023321 (2020).
- [150] J. U. Klamser, S. C. Kapfer, and W. Krauth, A kinetic-Monte Carlo perspective on active matter, *J. Chem. Phys.* **150**, 144113 (2019).
- [151] D. Rogel Rodriguez, F. Alarcon, R. Martinez, J. Ramirez, and C. Valeriani, Phase behaviour and dynamical features of a two-dimensional binary mixture of active/passive spherical particles, *Soft Matter* **16**, 1162 (2020).
- [152] V. Ramasubramani, B. D. Dice, E. S. Harper, M. P. Spellings, J. A. Anderson, and S. C. Glotzer, *freud*: A software suite for high throughput analysis of particle simulation data, *Comput. Phys. Commun.* **254**, 107275 (2020).
- [153] R. Gowers, M. Linke, J. Barnoud, T. Reddy, M. Melo, S. Seyler, J. Domański, D. Dotson, S. Buchoux, I. Kenney, *et al.*, MDAnalysis: A Python Package for the Rapid Analysis of Molecular Dynamics Simulations (2016) p. 98.
- [154] N. Michaud-Agrawal, E. J. Denning, T. B. Woolf, and O. Beckstein, MDAnalysis: A toolkit for the analysis of molecular dynamics simulations, *J. Comput. Chem.* **32**, 2319 (2011).
- [155] W. Humphrey, A. Dalke, and K. Schulten, VMD: Visual molecular dynamics, *J. Mol. Graph.* **14**, 33 (1996).
- [156] R. T. McGibbon, K. A. Beauchamp, M. P. Harrigan, C. Klein, J. M. Swails, C. X. Hernández, C. R. Schwantes, L.-P. Wang, T. J. Lane, and V. S. Pande, MDTraj: A Modern Open Library for the Analysis of Molecular Dynamics Trajectories, *Biophys. J.* **109**, 1528 (2015).
- [157] A. Stukowski, Visualization and analysis of atomistic simulation data with OVITO—the Open Visualization Tool, *Model. Simul. Mater. Sci. Eng.* **18**, 015012 (2010).
- [158] M. Sega, G. Hantal, B. Fábíán, and P. Jedlovský, Pytim: A python package for the interfacial analysis of molecular simulations, *J. Comput. Chem.* **39**, 2118 (2018).
- [159] T. Romo and A. Grossfield, LOOS: An extensible platform for the structural analysis of simulations (2009) p. 2332.
- [160] T. D. Romo, N. Leioatts, and A. Grossfield, Lightweight object oriented structure analysis: Tools for building tools to analyze molecular dynamics simulations, *J. Comput. Chem.* **35**, 2305 (2014).
- [161] K. Hinsen, The molecular modeling toolkit: A new approach to molecular simulations, *J. Comput. Chem.* **21**, 79 (2000).
- [162] The HDF Group, Hierarchical Data Format, version 5, <https://github.com/HDFGroup/hdf5>.
- [163] A. Collette, *Python and HDF5* (O'Reilly Media, Sebastopol, 2013).
- [164] P. de Buyl, P. H. Colberg, and F. Höfling, H5MD: A structured, efficient, and portable file format for molecular data, *Comput. Phys. Commun.* **185**, 1546 (2014).
- [165] W. M. Elhaddad and B. N. Alemdar, Efficient Management of Big Datasets Using HDF and SQLite: A Comparative Study Based on Building Simulation Data, in *Computing in Civil Engineering 2015* (2015) p. 249.
- [166] C. R. Harris, K. J. Millman, S. J. van der Walt, R. Gommers, P. Virtanen, D. Cournapeau, E. Wieser, J. Taylor, S. Berg, N. J. Smith, *et al.*, Array programming with NumPy, *Nature* **585**, 357 (2020).
- [167] S. van der Walt, S. C. Colbert, and G. Varoquaux, The NumPy Array: A Structure for Efficient Numerical Computation, *Comput. Sci. Eng.* **13**, 22 (2011).
- [168] P. Virtanen, R. Gommers, T. E. Oliphant, M. Haberland, T. Reddy, D. Cournapeau, E. Burovski, P. Peter-

- son, W. Weckesser, J. Bright, *et al.*, SciPy 1.0: fundamental algorithms for scientific computing in Python, *Nat. Methods* **17**, 261 (2020).
- [169] J. D. Hunter, Matplotlib: A 2D Graphics Environment, *Comput. Sci. Eng.* **9**, 90 (2007).
- [170] S. van der Walt, J. L. Schönberger, J. Nunez-Iglesias, F. Boulogne, J. D. Warner, N. Yager, E. Gouillart, and T. Yu, scikit-image: image processing in Python, *PeerJ* **2**, e453 (2014).
- [171] H. Löwen, Inertial effects of self-propelled particles: From active Brownian to active Langevin motion, *J. Chem. Phys.* **152**, 040901 (2020).
- [172] A. K. Omar, K. Klymko, T. GrandPre, and P. L. Geissler, Phase Diagram of Active Brownian Spheres: Crystallization and the Metastability of Motility-Induced Phase Separation, *Phys. Rev. Lett.* **126**, 188002 (2021).
- [173] A. P. Thompson, H. M. Aktulga, R. Berger, D. S. Bolintineanu, W. M. Brown, P. S. Crozier, P. J. in 't Veld, A. Kohlmeyer, S. G. Moore, T. D. Nguyen, *et al.*, LAMMPS - a flexible simulation tool for particle-based materials modeling at the atomic, meso, and continuum scales, *Comput. Phys. Commun.* **271**, 108171 (2022).
- [174] B. ten Hagen, S. van Teeffelen, and H. Löwen, Brownian motion of a self-propelled particle, *J. Phys. Condens. Matter* **23**, 194119 (2011).
- [175] J. D. Weeks, D. Chandler, and H. C. Andersen, Role of Repulsive Forces in Determining the Equilibrium Structure of Simple Liquids, *J. Chem. Phys.* **54**, 5237 (1971).
- [176] C. Scholz, S. Jahanshahi, A. Ldov, and H. Löwen, Inertial delay of self-propelled particles, *Nat. Commun.* **9**, 5156 (2018).
- [177] J. Su, Z. Cao, J. Wang, H. Jiang, and Z. Hou, Dynamical and thermodynamical origins of motility-induced phase separation, *Cell Reports Phys. Sci.* , 101817 (2024).
- [178] M. E. Cates and J. Tailleur, When are active Brownian particles and run-and-tumble particles equivalent? Consequences for motility-induced phase separation, *Europhys. Lett.* **101**, 20010 (2013).
- [179] J. U. Klamser, S. C. Kapfer, and W. Krauth, Thermodynamic phases in two-dimensional active matter, *Nat. Commun.* **9**, 5045 (2018).
- [180] C. W. Stewart and R. van der Ree, A Voronoi diagram based population model for social species of wildlife, *Ecol. Modell.* **221**, 1554 (2010).
- [181] C. Arcelli and G. Sanniti di Baja, Computing Voronoi diagrams in digital pictures, *Pattern Recognit. Lett.* **4**, 383 (1986).
- [182] L. Chen, G. Mukerjee, R. Dorfman, and S. M. Moghadas, Disease Risk Assessment Using a Voronoi-Based Network Analysis of Genes and Variants Scores, *Front. Genet.* **8**, 10.3389/fgene.2017.00029 (2017).
- [183] I. Vavilova, A. Elyiv, D. Dobrycheva, and O. Melnyk, The Voronoi Tessellation Method in Astronomy, in *Intell. Astrophys.* (Springer Nature Switzerland, Cham, 2021) p. 57.
- [184] H. Hu, X. Liu, and P. Hu, Voronoi diagram generation on the ellipsoidal earth, *Comput. Geosci.* **73**, 81 (2014).
- [185] F. Aurenhammer, Voronoi diagrams—a survey of a fundamental geometric data structure, *ACM Comput. Surv.* **23**, 345 (1991).
- [186] J. Burns, Centroidal Voronoi Tessellations, <http://www.whitman.edu/Documents/Academics/Mathematics/burns.pdf>, (accessed 2024-02-21).
- [187] D. R. Nelson, M. Rubinstein, and F. Spaepen, Order in two-dimensional binary random arrays, *Philos. Mag. A* **46**, 105 (1982).
- [188] L. F. Cugliandolo and G. Gonnella, Phases of active matter in two dimensions, arXiv:1810.11833 [cond-mat.stat-mech] (2018).
- [189] E. P. Bernard and W. Krauth, Two-Step Melting in Two Dimensions: First-Order Liquid-Hexatic Transition, *Phys. Rev. Lett.* **107**, 155704 (2011).
- [190] J.-P. Hansen and I. R. McDonald, *Theory of Simple Liquids*, 3rd ed. (Elsevier, Burlington, 2006).
- [191] V. M. Kendon, M. E. Cates, I. Pagonabarrage, J.-C. Desplat, and P. Bladon, Inertial effects in three-dimensional spinodal decomposition of a symmetric binary fluid mixture: a lattice Boltzmann study, *J. Fluid Mech.* **440**, 147 (2001).
- [192] Y. Zhang, A. Xu, G. Zhang, Y. Gan, Z. Chen, and S. Succi, Entropy production in thermal phase separation: a kinetic-theory approach, *Soft Matter* **15**, 2245 (2019).
- [193] S. Maneewongvatana and D. M. Mount, Analysis of approximate nearest neighbor searching with clustered point sets, arXiv:cs/9901013v1 [cs.CG] (1999).
- [194] D. Levis and L. Berthier, Clustering and heterogeneous dynamics in a kinetic Monte Carlo model of self-propelled hard disks, *Phys. Rev. E* **89**, 062301 (2014).
- [195] L. F. Cugliandolo, P. Digregorio, G. Gonnella, and A. Suma, Phase Coexistence in Two-Dimensional Passive and Active Dumbbell Systems, *Phys. Rev. Lett.* **119**, 268002 (2017).
- [196] F. Peruani, J. Starruß, V. Jakovljevic, L. Søgaard-Andersen, A. Deutsch, and M. Bär, Collective Motion and Nonequilibrium Cluster Formation in Colonies of Gliding Bacteria, *Phys. Rev. Lett.* **108**, 098102 (2012).
- [197] F. Peruani and M. Bär, A kinetic model and scaling properties of non-equilibrium clustering of self-propelled particles, *New J. Phys.* **15**, 065009 (2013).
- [198] G.-J. Liao and S. H. L. Klapp, Clustering and phase separation of circle swimmers dispersed in a monolayer, *Soft Matter* **14**, 7873 (2018).
- [199] R. C. Maloney, G.-J. Liao, S. H. L. Klapp, and C. K. Hall, Clustering and phase separation in mixtures of dipolar and active particles, *Soft Matter* **16**, 3779 (2020).
- [200] I. Palaia and A. Šarić, Controlling cluster size in 2D phase-separating binary mixtures with specific interactions, *J. Chem. Phys.* **156**, 194902 (2022).
- [201] F. Peruani, L. Schimansky-Geier, and M. Bär, Cluster dynamics and cluster size distributions in systems of self-propelled particles, *Eur. Phys. J. Spec. Top.* **191**, 173 (2010).
- [202] F. Peruani, A. Deutsch, and M. Bär, Nonequilibrium clustering of self-propelled rods, *Phys. Rev. E* **74**, 030904 (2006).
- [203] T. A. Witten and L. M. Sander, Diffusion-Limited Aggregation, a Kinetic Critical Phenomenon, *Phys. Rev. Lett.* **47**, 1400 (1981).
- [204] N. Kyriakopoulos, H. Chaté, and F. Ginelli, Clustering and anisotropic correlated percolation in polar flocks, *Phys. Rev. E* **100**, 022606 (2019).
- [205] M. Sanoria, R. Chelakkot, and A. Nandi, Percolation transition in phase-separating active fluid, *Phys. Rev. E* **106**, 034605 (2022).

- [206] S. Fehlinger and B. Liebchen, Collective behavior of active molecules: Dynamic clusters, holes, and active fractaltes, *Phys. Rev. Res.* **5**, L032038 (2023).
- [207] A. Ghosh, Z. Budrikis, V. Chikkadi, A. L. Sellerio, S. Zapperi, and P. Schall, Direct Observation of Percolation in the Yielding Transition of Colloidal Glasses, *Phys. Rev. Lett.* **118**, 148001 (2017).
- [208] D. Johansen, J. Trehella, and D. P. Goldenberg, Fractal dimension of an intrinsically disordered protein: Small-angle X-ray scattering and computational study of the bacteriophage λ N protein, *Protein Sci.* **20**, 1955 (2011).
- [209] A. M. Brasil, T. L. Farias, and M. G. Carvalho, Evaluation of the Fractal Properties of Cluster? Cluster Aggregates, *Aerosol Sci. Technol.* **33**, 440 (2000).
- [210] J. M. Tenti, S. N. Hernández Guiance, and I. M. Irurzun, Fractal dimension of diffusion-limited aggregation clusters grown on spherical surfaces, *Phys. Rev. E* **103**, 012138 (2021).
- [211] M. Tokuyama and K. Kawasaki, Fractal dimensions for diffusion-limited aggregation, *Phys. Lett. A* **100**, 337 (1984).
- [212] H. G. E. Hentschel, Fractal Dimension of Generalized Diffusion-Limited Aggregates, *Phys. Rev. Lett.* **52**, 212 (1984).
- [213] M. Paoluzzi, M. Leoni, and M. C. Marchetti, Fractal aggregation of active particles, *Phys. Rev. E* **98**, 052603 (2018).
- [214] L. Bai and D. Breen, Calculating Center of Mass in an Unbounded 2D Environment, *J. Graph. Tools* **13**, 53 (2008).
- [215] A. Bray, Theory of phase-ordering kinetics, *Adv. Phys.* **43**, 357 (1994).
- [216] K. Wu, E. Otoo, and A. Shoshani, Optimizing connected component labeling algorithms, in *Proc. SPIE 5747, Medical Imaging 2005: Image Processing* (2005) p. 1965.
- [217] C. Fiorio and J. Gustedt, Two linear time Union-Find strategies for image processing, *Theor. Comput. Sci.* **154**, 165 (1996).
- [218] R. Romero-Zaliz and J. Reinoso-Gordo, An Updated Review on Watershed Algorithms, in *Studies in Fuzziness and Soft Computing*, Vol. 358 (Springer Verlag, 2018) p. 235.